AD-A035 890 NAVAL POSTGRADUATE SCHOOL MONTEREY CALIF F/G 11/4
LOW ENERGY IMPACT LOADING OF GRAPHITE-EPOXY PLATES.(U)
DEC 76 R L FERRIS

UNCLASSIFIED NL

1 OF 2
ADA035890

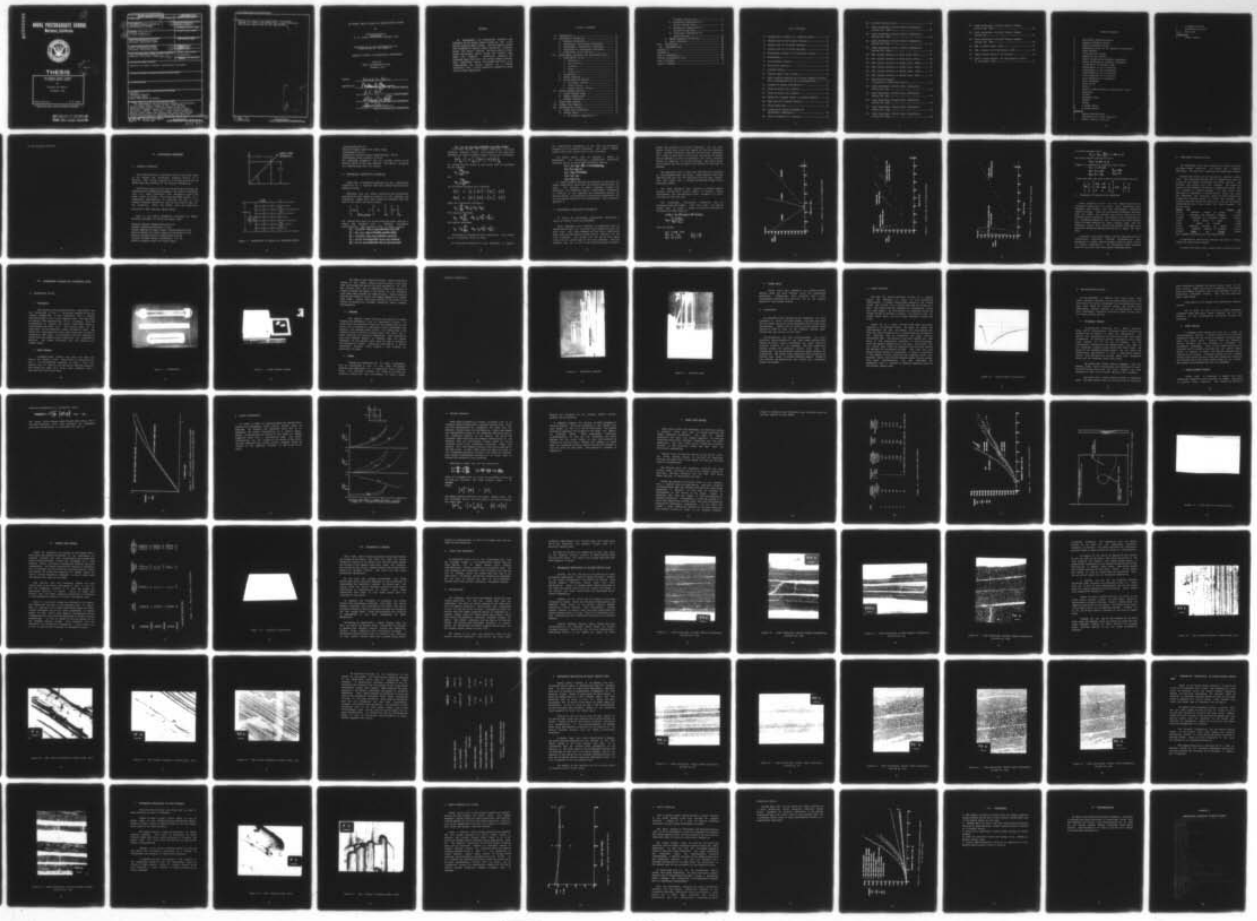

NAVAL POSTGRADUATE SCHOOL
Monterey, California

THESIS

LOW ENERGY IMPACT LOADING
OF GRAPHITE-EPOXY PLATES

by

Richard Lee Ferris

December 1976

Thesis Advisor: M. H. Bank

SECURITY CLASSIFICATION OF THIS PAGE (When Data Entered)

REPORT DOCUMENTATION PAGE

READ INSTRUCTIONS BEFORE COMPLETING FORM

1. REPORT NUMBER

2. GOVT ACCESSION NO.

3. RECIPIENT'S CATALOG NUMBER

4. TITLE (and Subtitle)
LOW ENERGY IMPACT LOADING OF GRAPHITE-EPOXY PLATES.

5. TYPE OF REPORT & PERIOD COVERED
Master's Thesis; December 1976

6. PERFORMING ORG. REPORT NUMBER

7. AUTHOR(s)
Richard Lee Ferris

8. CONTRACT OR GRANT NUMBER(s)

9. PERFORMING ORGANIZATION NAME AND ADDRESS
Naval Postgraduate School
Monterey, California 93940

10. PROGRAM ELEMENT, PROJECT, TASK AREA & WORK UNIT NUMBERS

11. CONTROLLING OFFICE NAME AND ADDRESS
Naval Postgraduate School
Monterey, California 93940

12. REPORT DATE
December 1976

13. NUMBER OF PAGES
105

14. MONITORING AGENCY NAME & ADDRESS(if different from Controlling Office)
Naval Postgraduate School
Monterey, California 93940

15. SECURITY CLASS. (of this report)
Unclassified

15a. DECLASSIFICATION/DOWNGRADING SCHEDULE

16. DISTRIBUTION STATEMENT (of this Report)

Approved for public release; distribution unlimited.

17. DISTRIBUTION STATEMENT (of the abstract entered in Block 20, if different from Report)

18. SUPPLEMENTARY NOTES

19. KEY WORDS (Continue on reverse side if necessary and identify by block number)
Laminate
Composite material
Low energy impact
Large deflections of plates

20. ABSTRACT (Continue on reverse side if necessary and identify by block number)

An experimental and theoretical analysis was performed on low energy impact loading of thin (.040 inches) graphite-epoxy plates. Six-inch square plates were subjected to dynamic impact (below the ballistic range) and static loading. The plate static strain energy and dynamic impact energy for failure were equal and constant. Theoretical analysis was performed using both exact and finite element methods. Small deflection theory was next page

DD FORM 1 JAN 73 1473 (Page 1)
EDITION OF 1 NOV 65 IS OBSOLETE
S/N 0102-014-6601

Unclassified
SECURITY CLASSIFICATION OF THIS PAGE (When Data Entered)

assumed and found to be inapplicable; the plates behaved in a manner indicating that a large deflection theoretical model would be more appropriate.

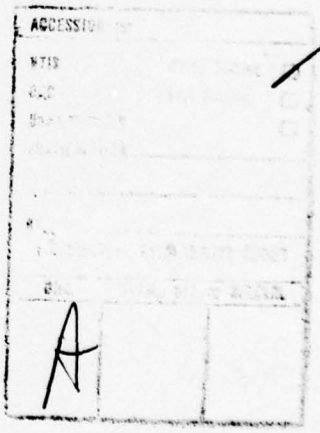

LOW ENERGY IMPACT LOADING OF GRAPHITE-EPOXY PLATES

by

Richard Lee Ferris
Lieutenant
B. S., United States Naval Academy, 1968

Submitted in partial fulfillment of the
requirements for the degree of

MASTER OF SCIENCE IN AERONAUTICAL ENGINEERING

from the
NAVAL POSTGRADUATE SCHOOL
December 1976

Author: Richard Lee Ferris

Approved by: Milton H. Bo
Thesis Advisor

R E Ball
Second Reader

Richard W. Ball
Chairman, Department of Aeronautics

Robert B. Brown
Dean of Science and Engineering

ABSTRACT

An experimental and theoretical analysis was performed on low energy impact loading of thin (.040 inches) graphite-epoxy plates. Six-inch square plates were subjected to dynamic impact (below the ballistic range) and static loading. The plate static strain energy and dynamic impact energy for failure were equal and constant. Theoretical analysis was performed using both exact and finite element methods. Small deflection theory was assumed and found to be inapplicable; the plates behaved in a manner indicating that a large deflection theoretical model would be more appropriate.

TABLE OF CONTENTS

LIST OF FIGURES

TABLE OF SYMBOLS

A	Extensional stiffness matrix
B	Coupling stiffness matrix
D	Bending stiffness matrix
E	Exponential power of 10, Modulus of elasticity
G	Shear modulus
N	Force per unit length
M	Moment per unit length
Q	Lamina stress-strain material properties
$\bar{Q}$	Lamina stress-strain material properties corrected to the plate's axes
U	Displacement in the X direction
V	Displacement in the Y direction
W	Displacement in the Z direction
a	Plate dimension in X direction
b	Plate dimension in Y direction
t	Plate thickness
γ	Shear strain
ϵ	Strain
θ	Angle of lamina fibers to the plate's X axis
κ	Curvature
μ	Microns
ν	Poisson's ratio
ρ	Density
σ	Stress
[]	A square matrix
{}	A column matrix

Subscript

K	Lamina identification
L	Longitudinal or fiber direction
ij	Matrix location i,j=1,2,3

s	A symmetric lay-up
T	Transverse direction
x,y,z	Plate axes

Superscript

o	Middle surface

I. INTRODUCTION

Composite materials have a tremendous potential in the structural field. Although their future value in the aircraft industry is exceptional, there still remain many unknowns. The response of graphite-epoxy composite plates to low energy impact loading is one of these unknowns.

Low energy impacts are a common occurrence on operational aircraft. A mechanic dropping a wrench, or a stone thrown by a tire are typical examples. It is important to know how composite panels react to these impacts in order to be able to confidently predict a damage threshold. An accurate model for damage would be helpful in both the operational and design fields. Operationally, the ability to assess damage to a panel which is known to have been hit, but which has no visual manifestations of damage, will produce better maintained and safer aircraft. The designer will also be better able to produce an aircraft capable of operation throughout its design environment.

A series of tests, both static and dynamic, were performed to analyze the response of a simply supported plate to impact loading. The plate was a symmetrically laid-up graphite-epoxy plate six inches square. The dynamic tests used a variable-mass steel penetrator of spherical shape, at impact speeds of ten, fifteen, and twenty feet per second. Each plate was impacted by incrementally increasing masses until failure occurred.

There were three basic types of failure expected. These included: static shear-out, where the penetrator sheared

through the panel causing only local damage; flexural, where the failure was caused primarily by bending and membrane stresses; and ballistic, where complete penetration occurred. It was assumed that wave stresses would have little influence, and that flexural failure would predominate. Small deflections were initially assumed and membrane stresses were neglected.

The Kirchoff Hypothesis for plates was adopted: straight lines normal to an undeformed middle surface were assumed to remain straight and normal to the middle surface in the deformed state. Further, it was assumed that normals to the middle surface do not change length.

The investigation proceeded in the following manner: first, the constitutive properties of the plate material were determined both analytically and experimentally, then the experimental apparatus was set up and calibrated to give the desired range of impact velocities. A number of non-destructive techniques for inspection of damaged plates were considered and tested. Finally, a series of static and impact tests was run, and the resulting damage was evaluated using both nondestructive and destructive test methods, including scanning-electron-microscopy.

Concurrently a theoretical investigation was undertaken to see whether simple linear theory could be of use in the analysis of the plate impact problem. Static and dynamic solutions were sought using SAP IV, a finite-element structural analysis program. Initially, known closed form solutions were compared with SAP IV solutions for static and dynamic loadings. Then specimen constitutive properties and experimental loading parameters were entered in the program, and solutions were compared with experimental data.

The procedures used and the results gained are detailed

in the following sections.

II. CONSTITUTIVE PROPERTIES

A. MATERIAL PROPERTIES

The plates used were constructed from 12 inch wide rolls of UCC Thornel 300 (untwisted) Graphite Fibers, in a Rigidite 5208 matrix, supplied as a B-stage prepreg by the NARMCO Materials Division of the Celanese Corporation.

Twelve-inch square panels were constructed following the manufacturers recommended procedures, and those of Linnander [Ref. 1]. These procedures were designed to give a 55% fiber content by volume. The lay-up was eight lamina in a symmetrical configuration as indicated by Fig. 1. The standard laminate orientation code for this lay-up [Ref. 2], was $(0,\pm45,0)_s$. After the proper cure, the panels were quartered to give six-inch square plates.

Some of the lamina properties predicted by NARMCO Materials included, in pounds per square inch:

Flexural modulus (longitudinal)=22.0 E6
Flexural modulus(transverse)= 1.6 E6
Tensile modulus of coupon sample (logitudinal)=20.5 E6
Tensile modulus for coupon sample (transverse)=1.47 E6
Flexural ultimate stress (longitudinal)=295 E3
Flexural ultimate stress (transverse)= 11.5 E3
Tensile ultimate stress for coupon sample

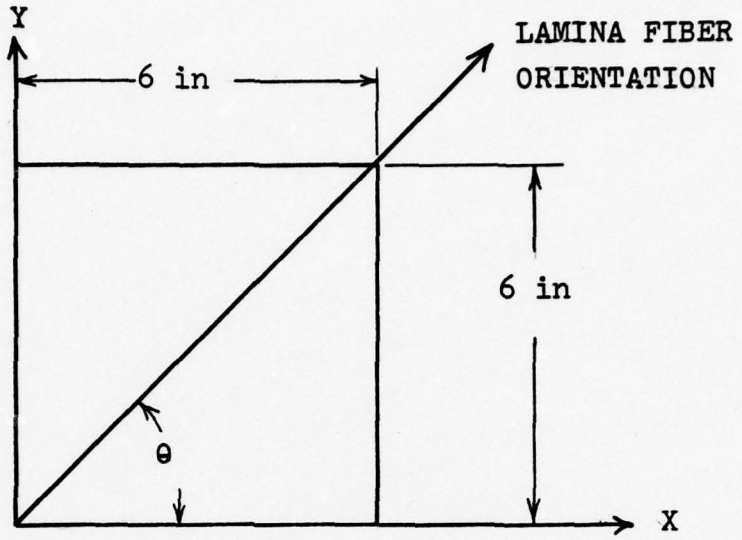

LAYER	θ
1	0
2	+45
3	-45
4	0
5	0
6	-45
7	+45
8	0

.040 in

.005 in

Figure 1 - ORIENTATION OF LAMINA ON A LAMINATED PLATE.

(longitudinal)=215 E3
Tensile ultimate stress for coupon sample
(transverse)=6.75 E3
Compression ultimate stress (longitudinal)= 198 E3
Interlaminar shear ultimate= 17.8 E3
The published properties did not include either of the Poisson ratios or the shear modulus. The nominal thickness of a laid-up plate was .040 inches.

B. THEORETICAL CONSTITUTIVE PROPERTIES

Jones [Ref. 3] developed equations for the constitutive properties of a laminate from known lamina properties and laminate lay-up.

Beginning with the known properties the constitutive properties of each lamina in relation to the laminate was determined. Lamina with fiber direction coincident with the axis of the plate; and plane stress:

$$\left\{ \sigma \right\}_{K^{th}\,LAYER} = \left[\quad Q \quad \right]_K \left\{ \varepsilon \right\}_K$$

For laminas that were not on the principle plate axis the Q matrix was modified with a suitable coordinate transformation. This applied to the ± 45 degree laminas:

$$\bar{Q}_{11} = Q_{11}\cos^4\theta + 2(Q_{12}+2Q_{66})\sin^2\theta\cos^2\theta + Q_{22}\sin^4\theta$$

$$\bar{Q}_{12} = (Q_{12}+Q_{22}-4Q_{66})\sin^2\theta\cos^2\theta + Q_{12}(\sin^4\theta+\cos^4\theta)$$

$$\bar{Q}_{22} = Q_{11}\sin^4\theta + 2(Q_{12}+2Q_{66})\sin^2\theta\cos^2\theta + Q_{22}\cos^4\theta$$

$$\bar{Q}_{16} = (Q_{11}-Q_{12}-2Q_{66})\sin\theta\cos^3\theta + (Q_{12}-Q_{22}+2Q_{66})\sin^3\theta\cos\theta$$

$$\bar{Q}_{26} = (Q_{11}-Q_{12}-2Q_{66})\sin^3\theta\cos\theta + (Q_{12}-Q_{22}+2Q_{66})\sin\theta\cos^3\theta$$

$$\bar{Q}_{66} = (Q_{11}+Q_{12}-2Q_{12}-2Q_{66})\sin^2\theta\cos^2\theta + Q_{66}(\sin^4\theta+\cos^4\theta)$$

For small strains and linear elasticity, utilizing classical laminate theory, the stresses in any layer were expressed in terms of middle surface strains and curvatures.

$$\{\sigma\}_K = [\,Q\,]_K \left\{ \{\varepsilon^\circ\} + z\{\chi\} \right\}_K$$

By integrating the stress in each lamina over the thickness of the laminate:

$$N_x \int_{-t/2}^{t/2} \sigma_x \, dz$$

and

$$M_x \int_{-t/2}^{t/2} \sigma_x z \, dz$$

the following relations were obtained:

$$\{N\} = [A]\{\varepsilon^\circ\} + [B]\{\chi\}$$

$$\{M\} = [B]\{\varepsilon^\circ\} + [D]\{\chi\}$$

where for extensional stiffness:

$$A_{ij} = \sum_{K=1}^{n} (\bar{Q}_{ij})_K (Z_K - Z_{K-1})$$

for coupling stiffness:

$$B_{ij} = 1/2 \sum_{K=1}^{n} (\bar{Q}_{ij})_K (Z_K^2 - Z_{K-1}^2)$$

for bending stiffness:

$$D_{ij} = 1/3 \sum_{K=1}^{n} (Q_{ij})_K (Z_K^3 - Z_{K-1}^3)$$

The plates as constructed were symmetrical. This forced the B, or coupling, matrix to zero.

To facilitate calculation it was desirable to express

the constitutive properties in the form of engineering constants of an orthotropic material. The finite element program used would accept data in this form only.

The Design Manual [Ref. 2] supplies a means to approximate the orthotropic constitutive properties utilizing the A, or extensional stiffness, matrix;

$$E_{xx} = (A_{11} A_{22} - A_{12}^2)/(\text{THICKNESS})A_{22}$$

$$E_{yy} = E_{xx} A_{22}/A_{11}$$

$$G_{xy} = A_{33}/\text{THICKNESS}$$

$$\nu_{yx} = A_{12}/A_{11}$$

$$\nu_{xy} = A_{22}/A_{12}$$

A simple computer program was designed to take both the lamina constitutive properties and laminate construction as input. The program, in Basic Language, outputs the following: the individual lamina stress-strain properties in relation to the laminate, the extensional matrix, the bending matrix, the orthotropic constitutive properties, and the orthotropic stress-strain relationship. This program is Appendix A.

C. EXPERIMENTAL CONSTITUTIVE PROPERTIES

To verify the calculated constitutive properties, a series of tensile tests was performed.

Three specimens were prepared in accordance with the design manual [Ref. 2]. They were nine inches long and one inch wide. The first specimen was cut from a twelve-inch panel with the zero degree fibers running parallel to the long dimension. The second was cut so the zero degree fibers ran at a right angle to the long dimension. The last specimen was cut so one of the forty-five degree lamina's

fibers were parallel to the long dimension, and the zero degree fibers were forty-five degrees off the long specimen axis. One-and-a-half-inch long and one-inch wide shoulders were glued to both sides of the outer one-and-a-half inches of the specimen in order to distribute the local stresses caused by mounting in the test machine. The edges, where the shoulders met the specimen, were beveled to less than 30 degrees.

BBH Electronics SR-4 strain gage rosettes were installed on each specimen near the center. These rosettes were type FAER-25R-12S6 with 120 ohm resistance and 2.04 gage factor. They were wired into a standard Wheatstone bridge strain measuring circuit.

The three specimens were mounted in a RIEHLE testing machine. As they were slowly loaded to failure, strain measurements were incrementally taken. Figures 2, 3, and 4 are plots of the test data.

The orthotropic constitutive properties can be determined from the graphs. From this data, the Design Manual [Ref. 2] gives a simple calculation procedure to determine the shear modulus:

$$U=(E_L+E_T+2\nu_{LT}E_Y)/8(1-\nu_{LT}\nu_{TL})$$

$$G_{LT}=\frac{2\,U\,E_X}{8U-E_X}$$

From the graphs:

$E_L = 11.65\ E6$
$E_T = 3.1\ E6$
$E_Y = 61.6\ E6$

$\nu_{LT} = .52$
$\nu_{TL} = .14$

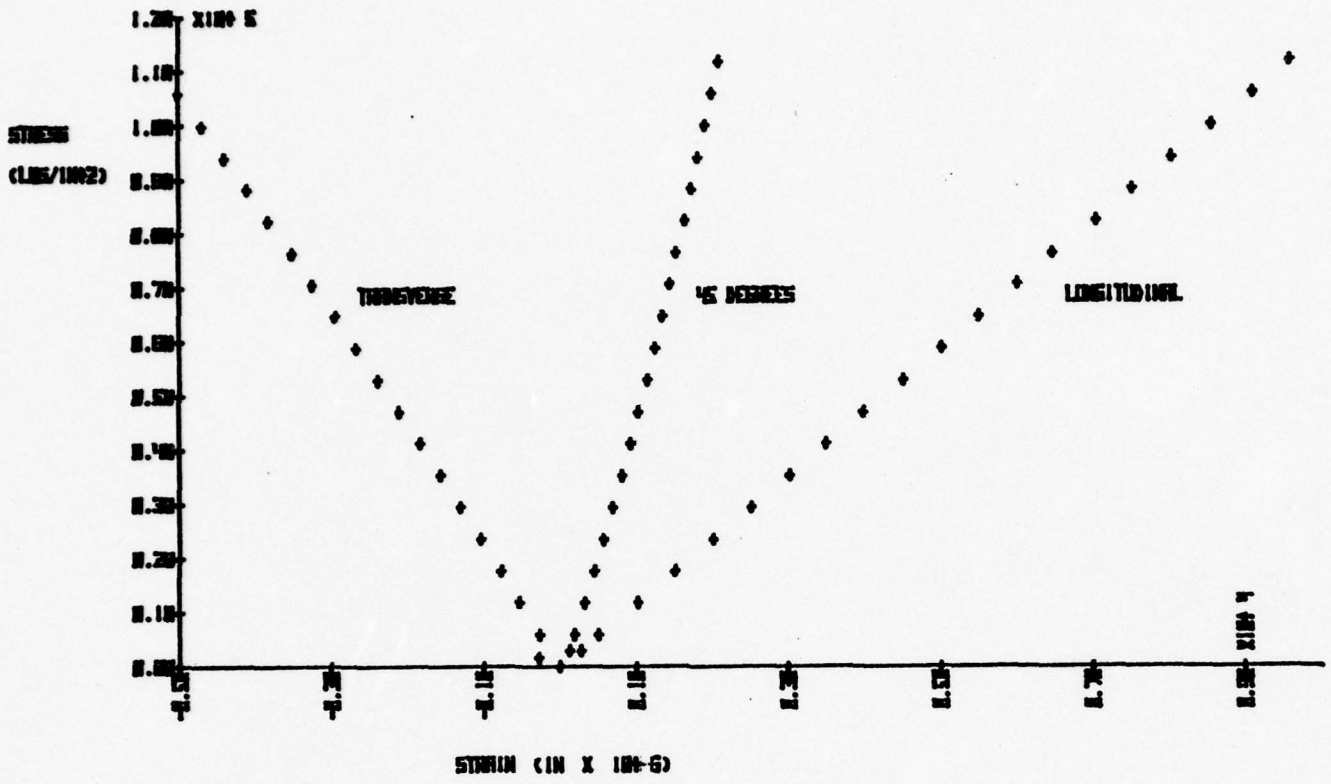

Figure 2 - TENSILE TEST OF ZERO DEGREE SPECIMEN

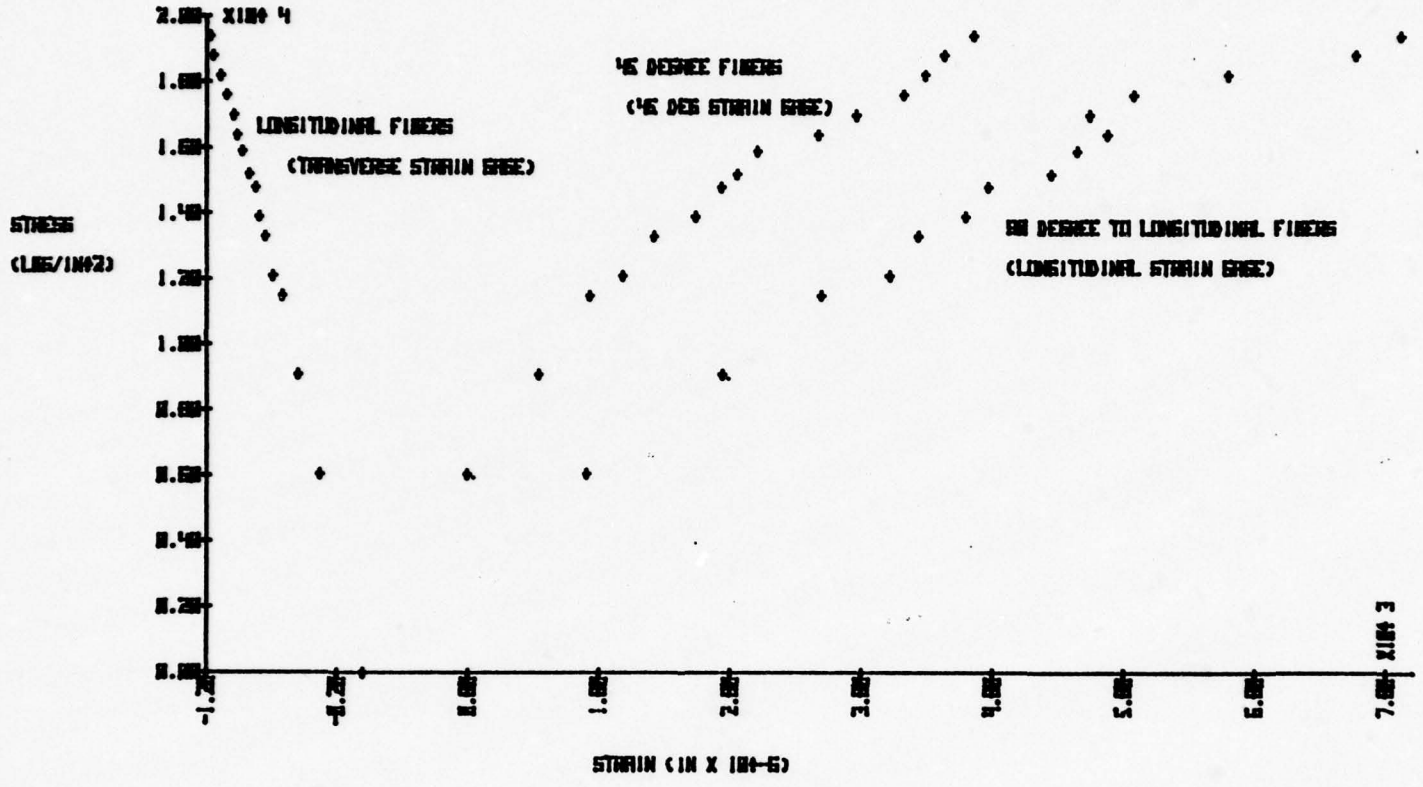

Figure 3 - TENSILE TEST OF 90 DEGREE SPECIMEN

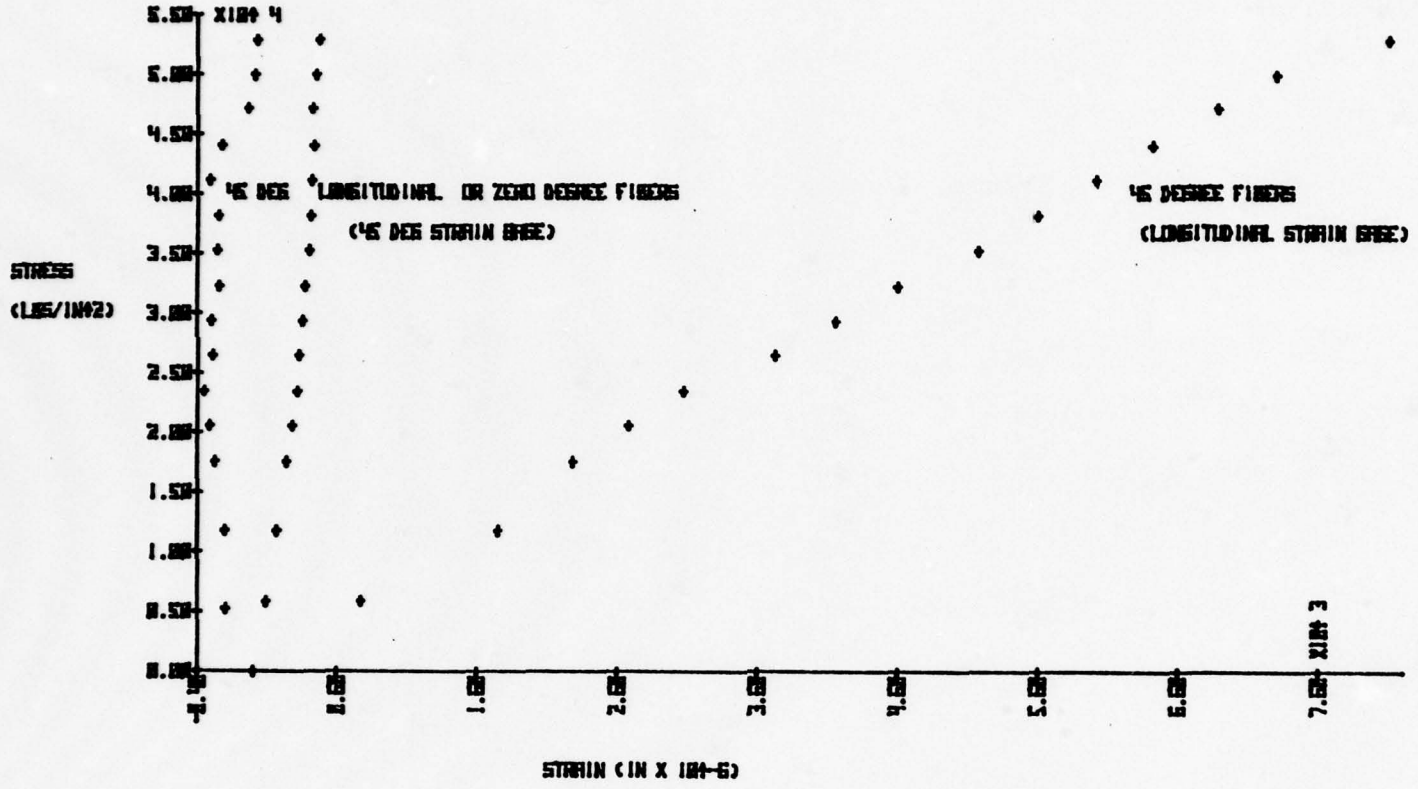

Figure 4 - TENSILE TEST OF 45 DEGREE SPECIMEN

To verify Poissons ratio:

$$\nu_{LT} = \nu_{TL} \left(\frac{E_T}{E_L}\right) = .138 \approx .14$$

The shear modulus calculation gave:

$$G_{LT} = 2.05 \text{ E } 6$$

Summary of constitutive properties from tests:

$$E_L = 11.6 \text{ E } 6 \qquad \nu_{LT} = .52$$
$$E_T = 3.1 \text{ E } 6 \qquad \nu_{TL} = .14$$
$$G_{LT} = 2.1 \text{ E } 6$$

Using this data the stress-strain relationships will be:

$$\left\{\sigma\right\} = \begin{bmatrix} 12.5 & 1.75 & 0 \\ 1.75 & 3.34 & 0 \\ 0 & 0 & 2.1 \end{bmatrix} \text{E } 6 \quad \left\{\varepsilon\right\}$$

D. COMPARISON OF CONSTITUTIVE PROPERTIES

Since Poisson's ratios and the shear modulus for an individual lamina were not given, these properties were estimated and entered into the constitutive properties computer program. Using the orthotropic properties obtained from the tests, the program was used to iterate for the unknown lamina properties. The results were disappointing. The calculated modulus in the Y direction was eight percent high, the shear modulus was forty percent high, and the Poisson's ratios were thirty five percent high when the X direction calculated modulus was forced to equal the test data.

A survey of the Design Manual [Ref.2] indicated that the constitutive properties obtained experimentally were comparable to common, medium strength graphite epoxy plates of similar construction. The orthotropic values obtained from the test data were used unless otherwise noted.

E. FIBER-EPOXY VOLUME FRACTION

Two independent tests were conducted to verify the fiber and epoxy volume fractions. One method was a chemical technique, the other was a quantitative microscopic method.

Handley and Cross [Ref.4] outlined the chemical method used. Two fritted crucibles and two samples were dried in an oven at 180 degrees centigrade for thirty minutes. The crucible and coupon were then weighed. The coupon was placed in 80-90 degree centigrade, concentrated nitric acid for fifteen to twenty minutes. The hot nitric acid dissolved or "digested" the epoxy matrix. After the epoxy was dissolved, the remaining fiber and acid solution was rinsed with a vacuum assist in water and acetone. The crucible with the fibers was dried in an oven at 120 degrees centigrade for one to two hours, and then weighed. The results were:

Sample One		Sample Two
1.0612	specimen weight in grams	1.3625
14.1733	specimen and crucible (before)	14.2385
13.9225	specimen and crucible (after)	13.9007
.2508	epoxy weight in grams	.3378
23.6%	epoxy by weight	24.8%
1.265	specific density of epoxy	1.265
1.9-2.3	specific density of graphite	1.9-2.3
64-68%	fiber by volume	63-67%

This compares favorably with the desired 65%.

A quantitative microscopic analysis was done to further verify the fiber/epoxy mixture.

A section was taken from a plate using a diamond cut-off

saw, and cold mounted in plastic. It was then polished using grinding belts of 50 and 320 grit, emory paper of 0 and 3/0 grit, and polishing cloths with aluminum-oxide slurries of 15 and .05 micrometer grit. The microstructure showed sufficient resolution with just polishing, so etching was not used. A nitric acid etch would have selectively attacked the epoxy, if desired. The cold mounting process caused slight sample degradation. The plastic attacked the epoxy in the outermost layer. The attack was very slight and confined to dissolving the extreme surface layer of epoxy. If there was a well developed crack, the plastic would also fill these with a corresponding light attack on the surrounding matrix material. The plastic mounting material was also significantly softer than the graphite epoxy plate making it difficult to obtain square edges on the sample.

Figure 5 details the results of the quantitative analysis. The illustration is the 300X microphotograph used for the analysis, which is a picture of the middle two layers of a plate. The data indicates a fractional length of line within the fiber as .557. This equates to the volume fraction giving a 55.7% fiber volume, which concurs with previous analysis.

The average dimension of the fibers was also determined from the microphotograph using standard quantitative microscopy techniques. The average dimension was 5.4 microns. Since the specimen was cut at a right angle to the principle fiber orientation, this dimension gives a close approximation of the average fiber diameter.

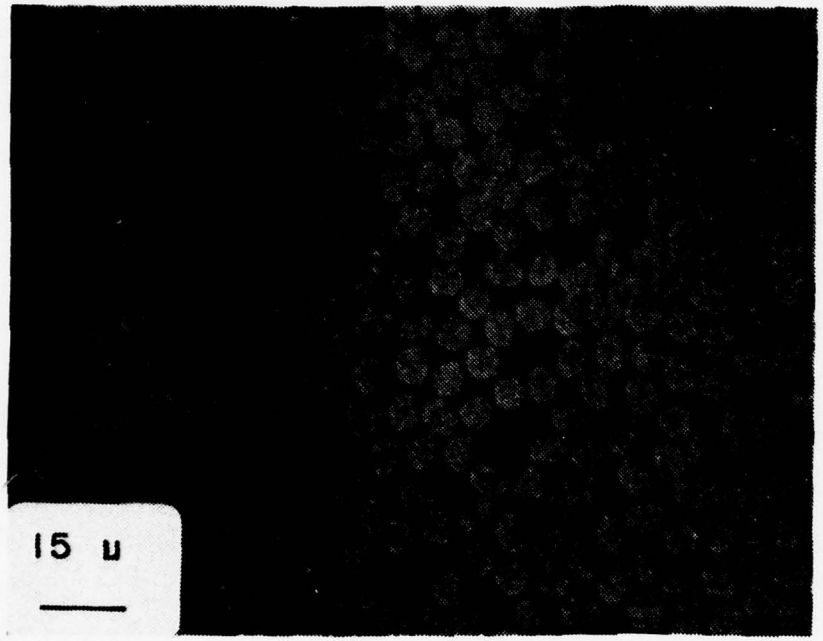

Random line number	Line length in mm	Fiber length in mm	# of fibers	% fibers
1	8.9	5.46	14	61.3
2	8.9	6.0	14	67.4
3	8.9	6.55	14	73.6
4	11.41	5.6	13	62.9
5	11.41	7.18	18	62.9
6	11.41	7.5	17	65.7
7	11.41	7.6	17	66.6
TOTAL	69.83	45.89	107	65.7

Figure 5 - MICROSCOPIC ANALYSIS OF FIBER-VOLUME CONTENT

III. EXPERIMENTAL APPARATUS AND PRELIMINARY TESTS

A. EXPERIMENTAL SET-UP

1. Penetrator

Two variable mass penetrators were constructed and are illustrated in Fig. 6. The primary penetrator was the lighter, slimmer one. It was constructed with a plastic pipe body sized to fit in the launcher tube. The mass could be adjusted from approximently .014 to .093 slugs. This was accomplished by varying the weight from seven ounces to three pounds with lead shot. The leading point of the penetrator is half-spherical shaped and made of steel. The larger all steel penetrator had a mass which could be varied starting at .085 slugs. This penetrator had the capacity to change both the leading point's shape and its construction material. The second penetrator was not needed in the dynamic tests.

2. Plate Fixture

A massive steel fixture was built for both the static and dynamic tests. This fixture is illustrated in Fig. 7. It was carefully machined to have a flat test surface and to have the top and bottom surfaces parallel. The fixture was made from heavy steel channels with a one-half-inch thick steel base.

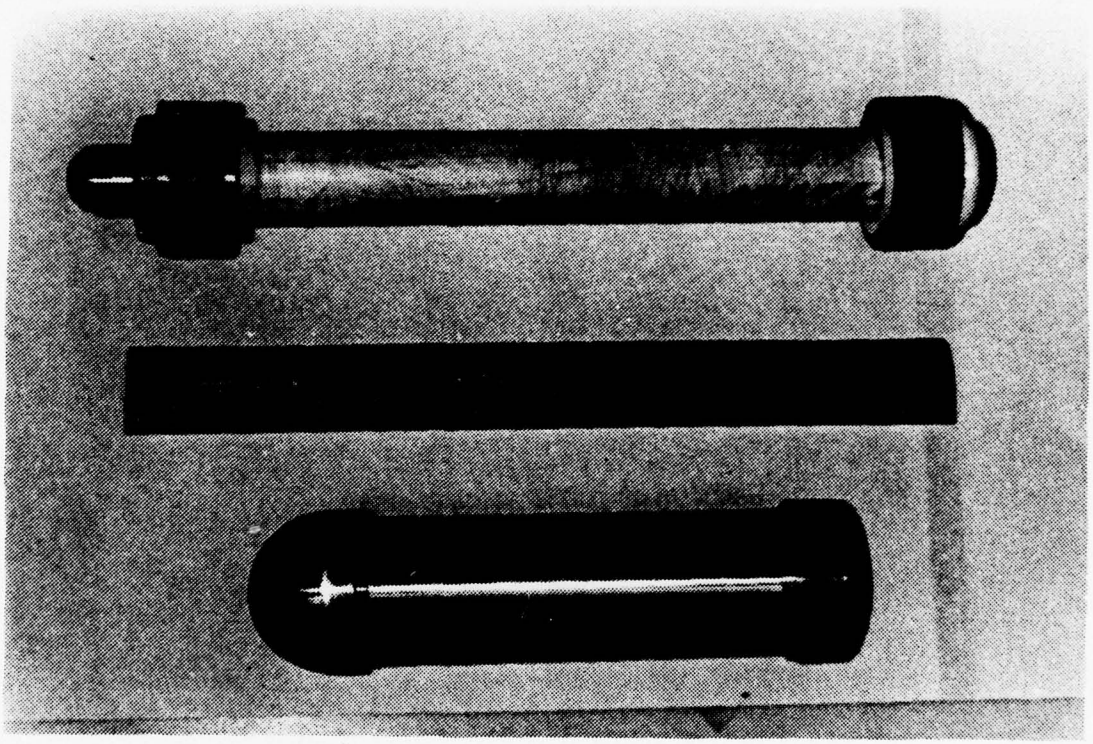

Figure 6 - PENETRATORS

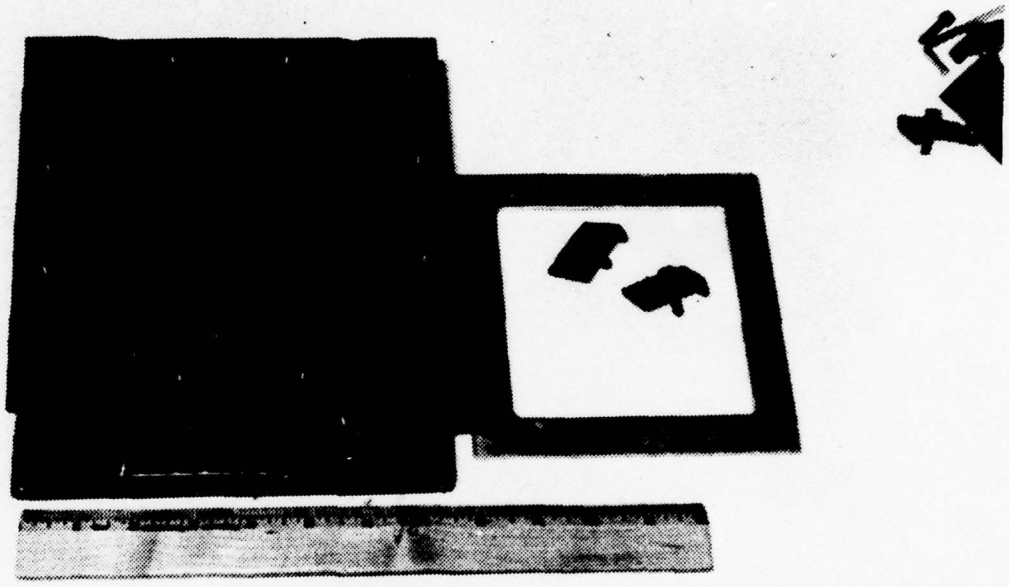

Figure 7 - PLATE TESTING FIXTURE

The square test supports measured four-and-one-half inches on the inside. Using a six-inch plate, each plate edge over-lapped the support by three quarters of an inch. The fixture also had an additional frame and a series of clamps to secure all edges of the plates to the fixtures; this frame would prevent all edge rotation. Plates could be mounted and tested in either the simply supported or clamped edge modes. Large holes were drilled in the sides of the fixture to prevent any pressure build-ups during dynamic displacements.

3. Launcher

The desired impact velocity was achieved by simply dropping the penetrator from an appropriate height. To insure that the penetrator would hit the desired spot on the plate, and to provide for repeatable, easily adjustable drop heights, the launcher shown in Fig. 8 was constructed. The launcher could be varied in height above the plate via a screw crank for fine velocity adjustments. Both penetrators were just slightly smaller in diameter than the inside dimension of the launcher tube, which was used to stabilize the penetrator's flight. Launch was initiated by a switch controlled solenoid which removed a bar holding the penetrator in place.

4. Frame

A frame was constructed out of steel scaffolding, and is illustrated in Fig. 9. The frame was plumbed vertical and constructed on a heavy-load rated concrete floor. The launcher assembly was moved up and down the frame by a pulley and rope arrangement to obtain course

velocity adjustments.

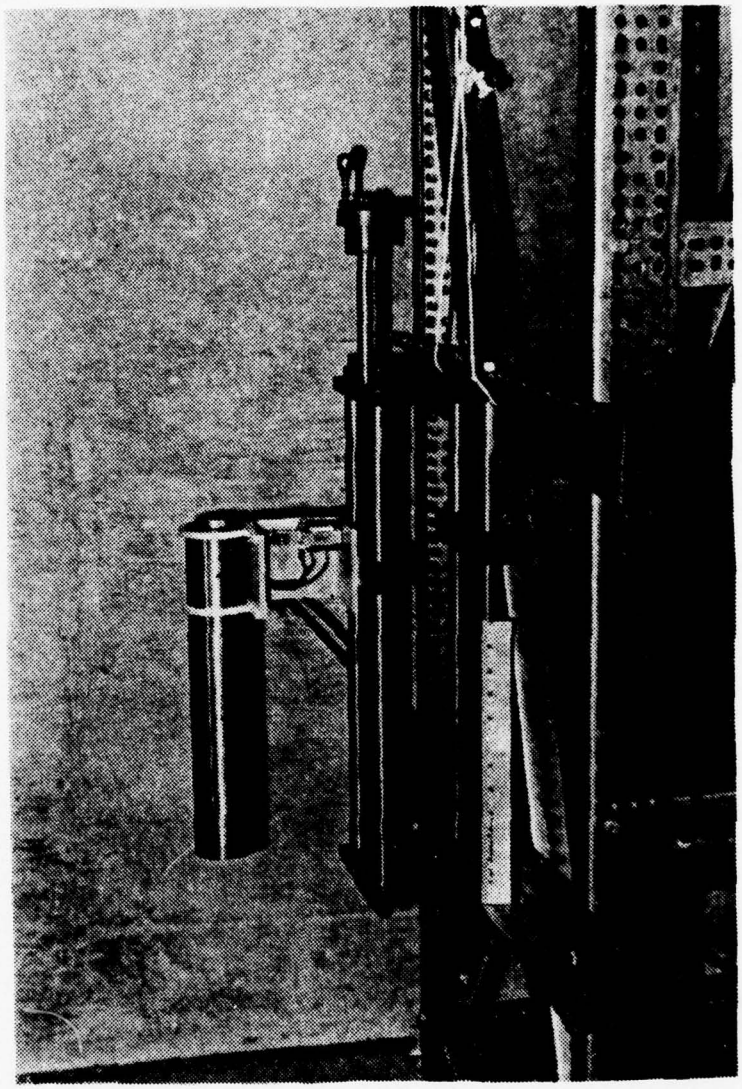

Figure 3 - PENETRATOR LAUNCHER

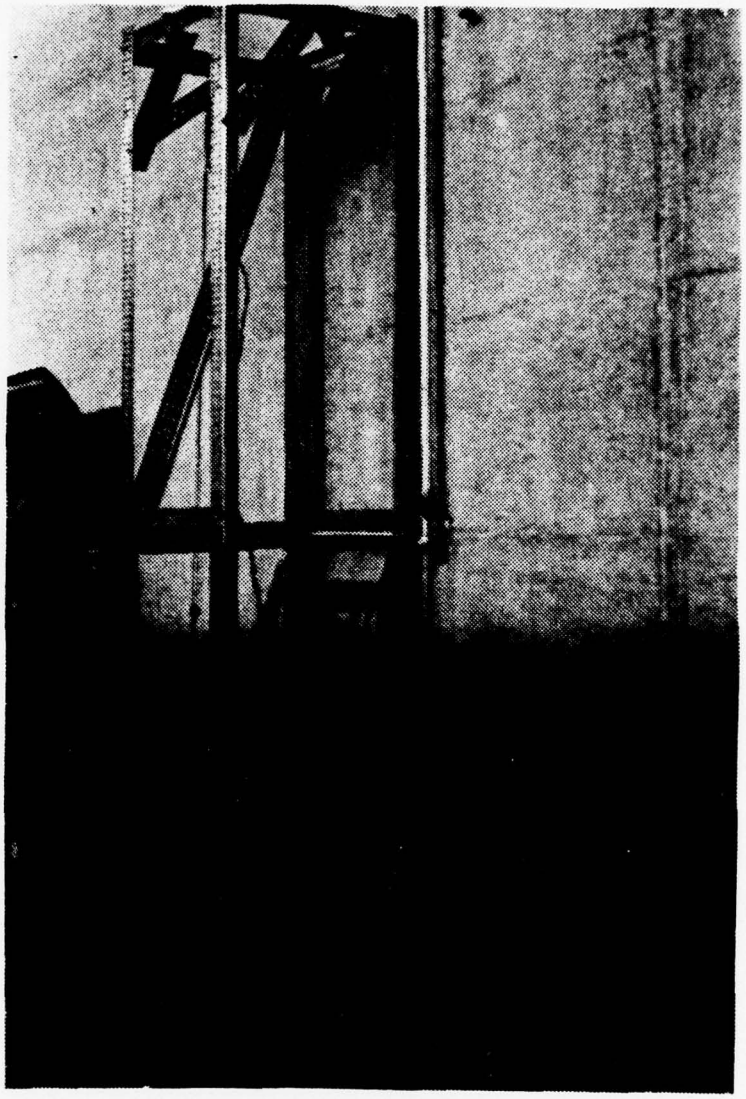

Figure 9 - LAUNCHER FRAME

5. Static Tests

Static tests were conducted on a RIEHLE testing machine using the base fixture, plate and appropriate penetrator. Deflections were measured with a dial displacement indicator from the cross arm of the testing machine to the working surface.

B. CALIBRATION

The launcher-frame combination was calibrated for both impactors at three different speeds. Ten feet per second was the lowest practical speed obtainable due to launch tube interference. Twenty feet per second was the highest speed desired in order to keep in the flexural failure mode. Fifteen feet per second was also used.

The calibration was done electronically. Two light sensitive photo-transistors and their power supplies were placed two inches apart, bracketing the plate fixture's position relative to the launcher. Two light beams were focused across the penetrator flight path onto the transistors, and an electronic timer was placed between the transistors. The wooden frame supporting this apparatus was painted flat black to prevent spurious imputs. Speeds of ten, fifteen, and twenty feet per second were calibrated within two percent.

C. IMPACT DURATION

The time and strain-amplitude history of a typical impact was obtained to assist in the theoretical calculations. A graphite epoxy plate similar to the tested plates was fitted with a strain gage near the center of a face. The strain gage was connected to a Wheatstone bridge and power supply. An oscilloscope was connected across the bridge and set to trigger on impact. The scope was set for single sweep mode, and had a camera mounted to record the trace.

Figure 10 is a scope picture taken using the larger impactor at its lightest weight. The speed of impact was approximately ten feet per second. The oscilloscope time scale for this photograph was .5 miliseconds per centimeter. The amplitude was not calibrated and gives relative information only. The strain in the plate reached its peak value at one millisecond according to this photograph. After the impact, examination of the plate determined that the strain gage leads had separated from the gage leaving the validity of the results in doubt. The test did give several useful pieces of information. It gave an indication of the impact's initial shape and rise time,and, since wave stresses would have reached maximum values in much quicker time ranges (microseconds), the test confirmed the assumption that a flexural or membrane mechanism would be the primary loading mode.

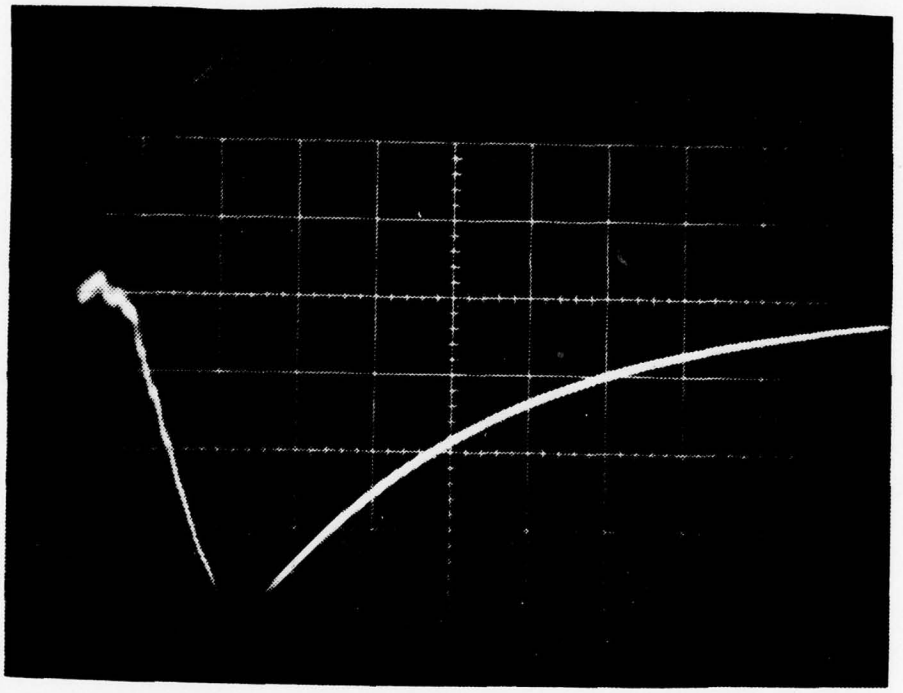

Figure 10 - TYPICAL IMPACT TIME HISTORY

D. NON-DESTRUCTIVE TESTING

It was necessary to examine each plate after every impact loading to determine if any damage had occurred. The tests had to be quick, inexpensive and non-destructive since many tests would be required during the course of the experiments. Several methods of non-destructive testing were considered, including: ultrasonic sound, X-rays, and a new liquid crystal process.

1. Ultrasonic Testing

An Automation Industries Inc., Sperry Division, Model UM-771 Reflectoscope Ultrasonic Testing Machine was examined for its ability to meet the requirements. The machine was equipped with 2.25 MHz and 5.0 MHz zero degree transducers. It also had 2.25 MHz transducers with sound input angles of 45, 60, and 90 degrees. All the transducers, including various combinations, were used on two different graphite epoxy panels with known flaws. One panel had the standard surface finish, and the other was specifically manufactured to give a very smooth surface finish. Both the shear and through modes were attempted, along with the different angle input modes.

The panels with normal surface roughness, from the bleeder plies used in manufacture, were difficult to test. The sound return from both the front (input), and back surfaces was lost in the clutter caused by the roughness.

The plate with a smooth surface allowed a reasonable input and back surface echo, but the plate was so thin that

these reflections occupied the entire useful range of the echo returns. Known flaws could be detected in the clutter using the highest frequency, but it was difficult to get any continuous, consistent returns. This was true even with known, large flaws.

Other modes of the machine were tested with negative results.

For a plate as thin as this, a higher frequency transducer might have given useful results, but for the purposes of this investigation ultrasonic testing was discarded.

2. X-Ray Testing

A portable X-Ray Machine was tried as a means of non-destructive testing. A General Electric LX-40 Portable Industrial X-Ray Unit was set-up to examine a graphite epoxy panel with known flaws. Polaroid film was exposed at various kilovolt and time settings to determine the procedure's usefulness. Even at the lowest setting of 70 kilovolts and 10 seconds, the plate did not absorb enough energy to produce an image. The pictures obtained had no contrast and no detail. A machine capable of even smaller energy output would probably still have difficulty obtaining any contrast due to the light atomic weight of the carbon. This means of non-destructive test was abandoned.

3. Liquid Crystal Testing

Shaum [Ref. 5] developed a method for using temperature sensitive liquid crystals for damage evaluation in graphite epoxy laminates. This method was used with

excellent results.

After preparing plates for testing, they were painted flat black on one side. Liquid crystals, with temperature sensitivity of 30±1 degrees centigrade, were mixed with water and a small quantity of wetting compound (liquid detergent). This mixture was then spray painted on the plate to be tested.

After each impact during the dynamic testing, the plate was examined for damage. This was accomplished by selectively heating all, or just a portion, of the panel, and watching the heat transfer cause the liquid crystals to change color. Any damaged area would experience a different heat transfer rate and thus would change color at a different time from an undamaged part. This method was sensitive enough to show even slight compressive indentations in the surface prior to their becoming visually or tactually evident.

IV. FINITE ELEMENT ANALYSIS

A. FINITE ELEMENT MODEL

SAP IV, a structural analysis program for static and dynamic response of linear systems by Bathe, Wilson and Peterson [Ref. 6] was used as an analytical tool.

Two finite element models of a plate were made for analysis. The first model was a coarse model consisting of only 16 square plate elements, 1.125 inches on a side, for a 4.5 inch square plate. This model was used for initial "coarse" investigation at a small cost in computer time. The second model was a fine model with 324 plate elements, .25 inches square, and used considerable computer time.

The results produced by SAP IV using these models were compared with known, exact solutions for aluminum plates. Timoshenko and Woinowsky-Krieger [Ref. 7] solved the simply supported, concentrated load problem, which was used as the reference solution. Figure 11 shows a plot of the deflection versus position on a plate (from an edge to the center keeping Y constant) under a 100 pound load. The fine finite element model is .4% stiffer than the exact solution, where the coarse model is 5.5% stiffer than the exact solution.

The dynamic analysis section of SAP was addressed to compare its modal frequency with an exact solution. Meirovitch [Ref. 8] gives an exact solution for the

vibration frequencies of a rectangular plate:

$$\text{FREQUENCY} = \pi^2 \sqrt{\frac{D}{\rho}} \left[\left(\frac{m}{a}\right)^2 + \left(\frac{n}{b}\right)^2 \right] \qquad m,n = 1,2,\ldots$$

The coarse finite element model results were within .5% of the exact solution. Since this agreement was considered more than satisfactory, the fine model was not run.

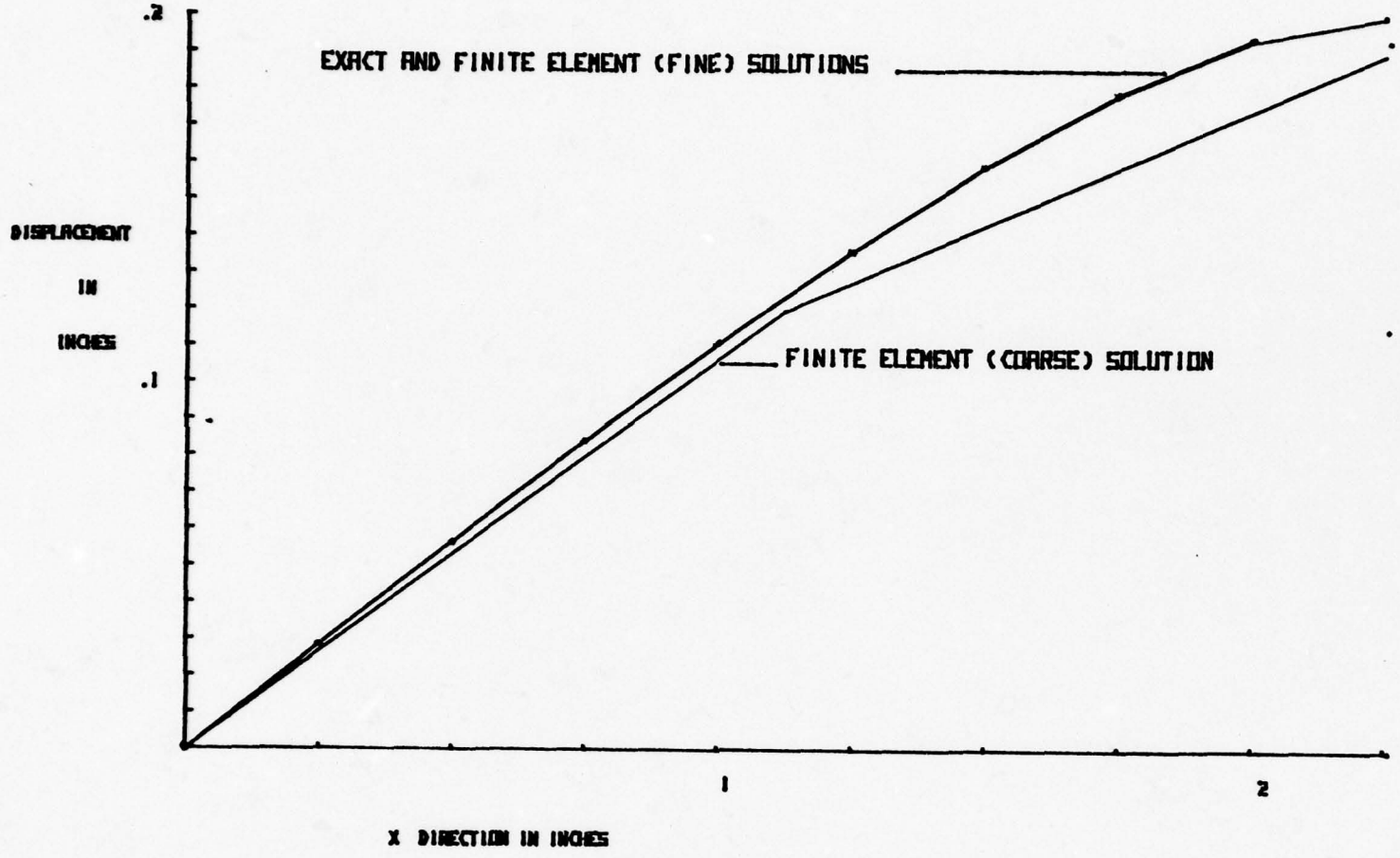

Figure 11 - EXACT SOLUTION COMPARED WITH FINITE ELEMENT SOLUTIONS FOR A CONCENTRATED LOAD ON AN ALUMINUM PLATE

B. STRESS DISTRIBUTION

In order to limit the required amount of computer data reduction by determining where initial failure could be expected, an analysis was performed using SAP IV to determine the stress distribution on a typical plate. Figure 12 illustrates the results of this study on a simply supported plate with a concentrated load. The stress concentration was the highest at the center of the plate, and this indicated that initial failure analysis could be limited to the immediate vicinity of the center of the plate.

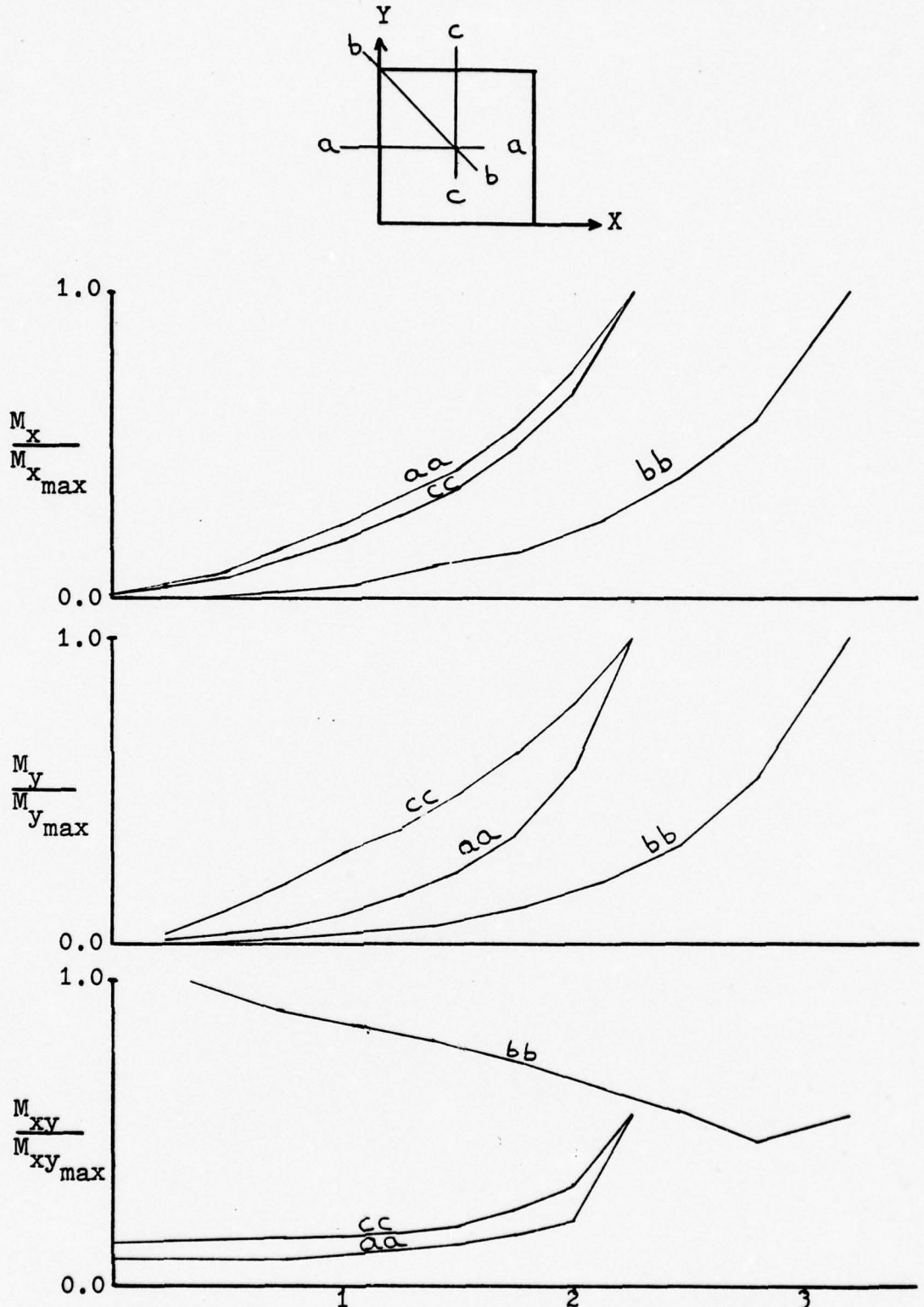

Figure 12 - DIAGRAM OF STRESS DISTRIBUTION

C. FAILURE CRITERION

Tests made by McQuillen, Llorens, and Gause [Ref. 9] on composite beams demonstrated a flexural failure mode. Thus, for this investigation the assumption was made that the flexural failure mode would predominate. Since each lamina was significantly weaker in the transverse direction than in the direction parallel to the fibers, and since the outermost layer would have the highest stress level, it was expected that the preliminary failure would be in the outermost layer in the transverse direction. After this failure, the load normally carried would be transferred to the next layer. If this lamina could not carry the load in its transverse direction, failure of the plate was assumed. Each lamina's longitudinal strength was so large that no failure was allowed in that direction.

Returning to Jones [Ref. 3], the strains are:

$$\epsilon_x = \frac{\partial u_0}{\partial x} - z\frac{\partial^2 w_0}{\partial x^2} \qquad \gamma_{xy} = \frac{\partial u_0}{\partial y} + \frac{\partial v_0}{\partial x} - 2z\frac{\partial^2 w_0}{\partial x \partial y}$$

$$\epsilon_y = \frac{\partial v_0}{\partial y} - z\frac{\partial^2 w_0}{\partial x^2}$$

Since it is assumed that the length of the middle surface of the plate is constant, the first partial terms can be dropped.

Using,

$$[D]^{-1}\{M\} = \{\kappa\}$$

the middle surface curvatures are found. Having these, and the stiffness matrix for each lamina, the lamina stresses are found from:

$$\{\sigma\}_K = [Q]_K\{\epsilon\}_K \qquad \{\epsilon\} = z\{\kappa\}$$

Knowing the stresses and the ultimate failure stress, failure can be predicted.

A computer program was written in Basic Language to evaluate failure. The input consisted of the moments per unit length in the X, Y, and XY directions. The program started by computing the stresses in the outer two layers, as outlined above, using appropriate coordinate transformations. It then set the transverse and shear modulus for the outer lamina to zero and computed the stresses on the next layer. Failure was assumed to occur when the transverse ultimate failure stress was exceeded in both the outer and next layer. The program is included as Appendix B.

V. STATIC TEST RESULTS

Seven static tests were performed, six involving loading to failure. Three tests used the larger penetrator and simply supported boundaries. Two used the smaller penetrator and were also simply supported. One test was conducted using fixed boundary conditions and the small penetrator. The last plate was not loaded until failure; instead, it was partially loaded and then used for microscopic examination.

Figures 13 and 14 show the results of all static tests. The static failure energy, as outlined by McQuillen, Llorens, and Gause [Ref. 9] for beams, was one half the load times the displacement.

All failures, with one exception, involved the same failure mode, and Figure 15 and 16 are typical examples of this mode. The only exception was the test with fixed edges, and Fig. 17 illustrates its mode.

During the course of the static tests it was apparent that a "yield" point was experienced. This point occurred at approximately half the ultimate load when the panel would experience a decrease in load with no increase in displacement at the center of the plate. Figure 14 indicates that this was common to both penetrators and boundary conditions. Consequently, a plate was loaded to a point just beyond this "yield" point, and then sectioned and prepared for microscopic examination. As the plate was loaded a large deflection occurred in the plate which was very similar in size and shape to the standard failure.

Figure 18 indicates this deflection area, and shows were the sections (marked 5) were taken.

TEST	BOUNDARY CONDITIONS ss = simply supported f = fixed	PENETRATOR SIZE s = small l = large	ULTIMATE DISPLACEMENT OF CENTER OF PLATE (inches)	ULTIMATE LOAD (lbs)	ULTIMATE ENERGY ½(disp)(load) (ft-lbs)
1	ss	l	.337	305	4.28
2	ss	l	.38	350	5.54
3	ss	l	.396	345	5.61
4	ss	s	.385	265	4.25
5	ss	s	.356	295	4.37
6	f	s	≐.255	≐380	≐4
7	ss	l not loaded until failure		-max load=190	-max disp=.222

Figure 13 - TABLE OF STATIC TEST RESULTS

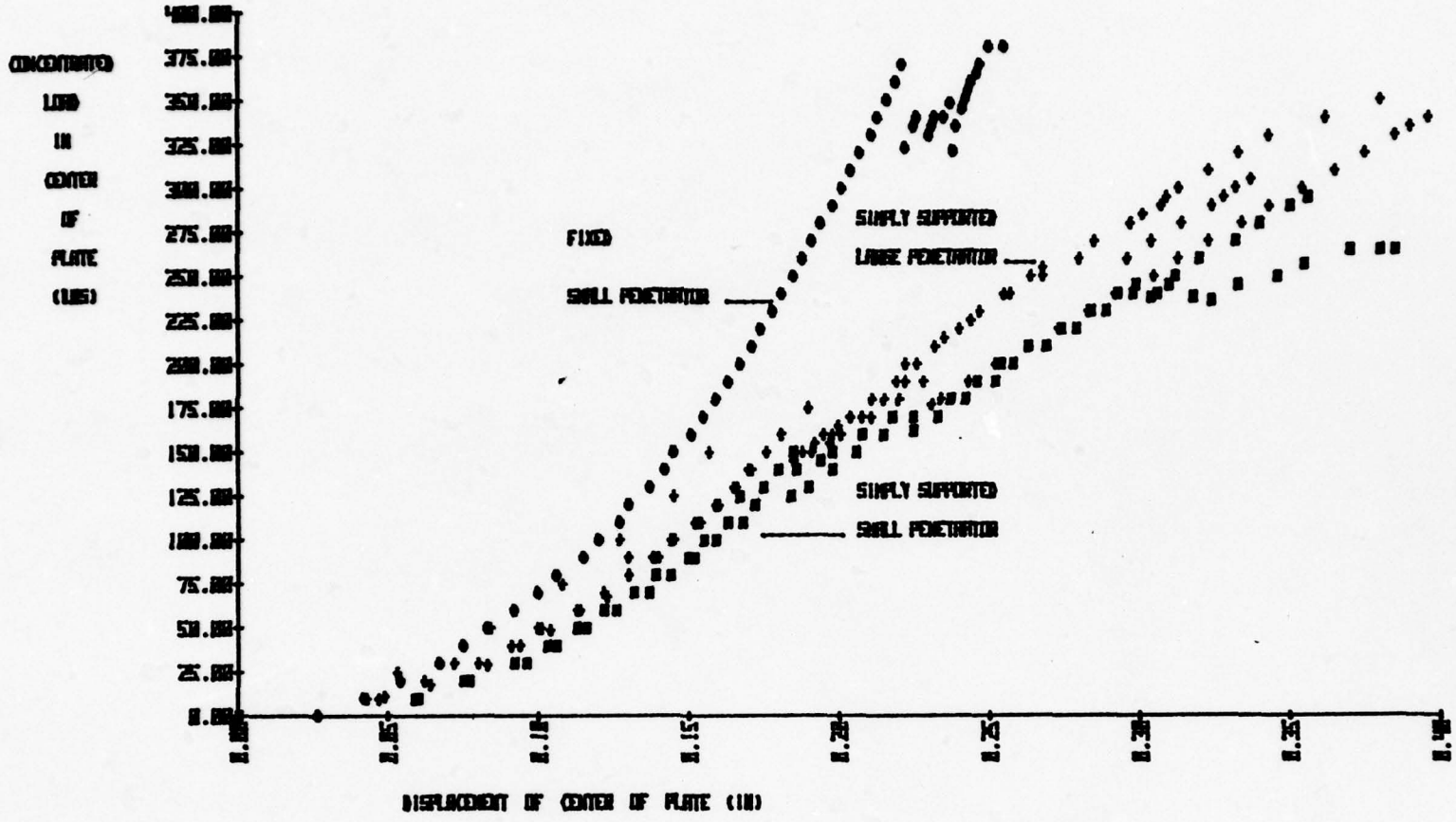

Figure 14 - GRAPH OF STATIC TEST RESULTS

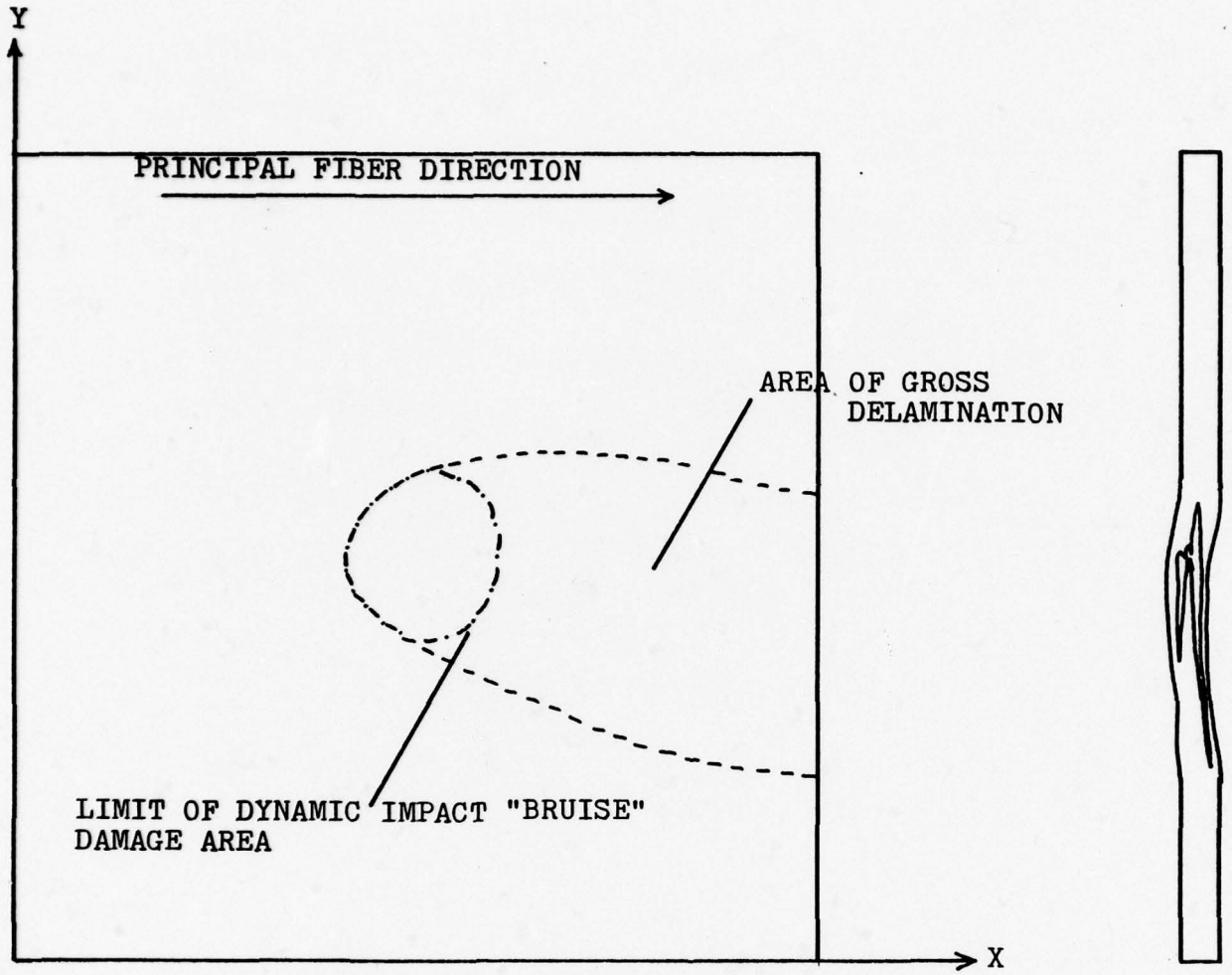

Figure 15 - SKETCH OF A TYPICAL STATIC OR DYNAMIC FAILURE

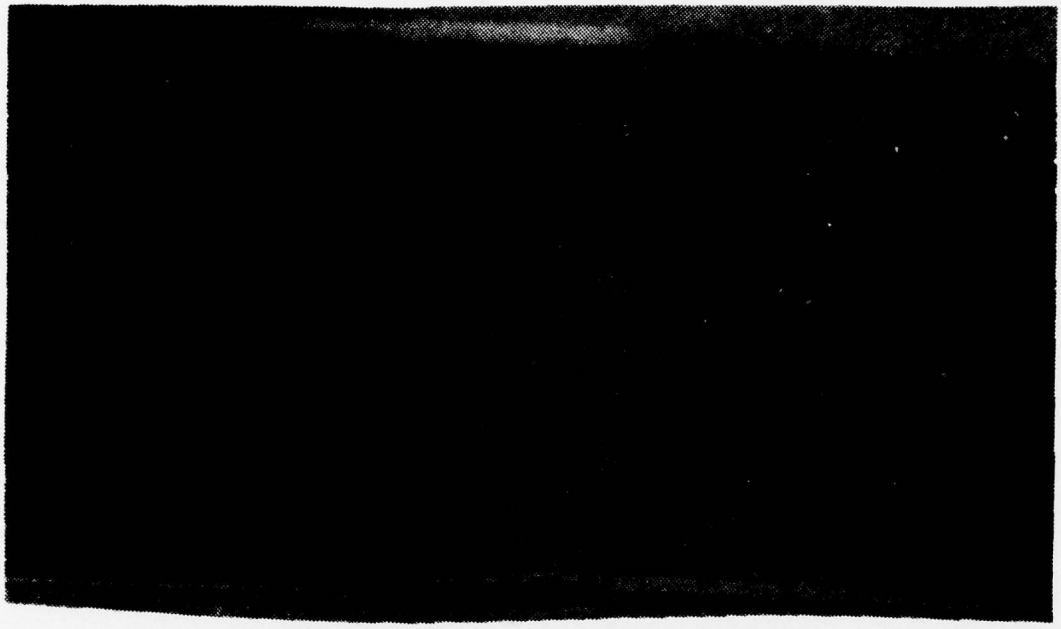

Figure 16 - EDGE VIEW OF A TYPICAL FAILURE

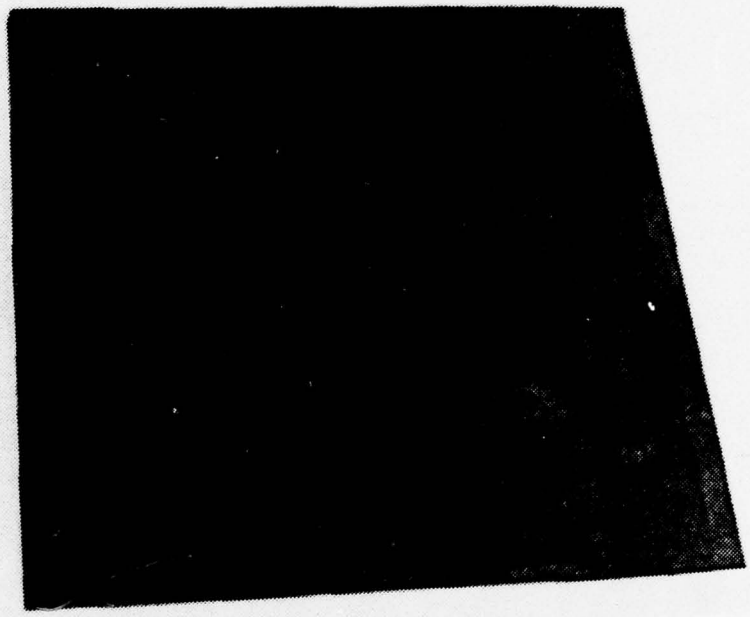

Figure 17 - STATIC SHEAR-OUT

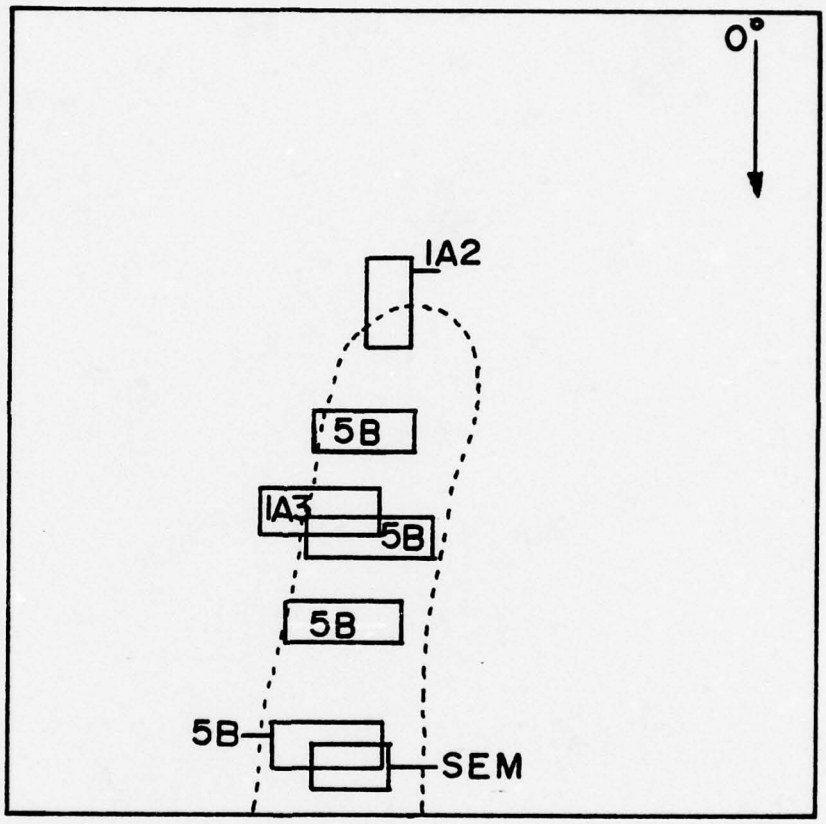

Figure 18 - LOCATIONS OF SECTIONS REMOVED FOR MICROSCOPIC EXAMINATION

VI. DYNAMIC TEST RESULTS

Figure 19 summarizes the results of the dynamic tests. Each plate was impacted repeatedly by the penetrator, at constant velocity but with progressively increasing mass until failure occurred. Failure was evidenced by a loud cracking noise, virtually no penetrator rebound, and gross delamination. The energy required for failure is indicated, and is one-half the mass times the velocity squared. After each impact the plates were examined for damage using the liquid crystal inspection technique. In all of these tests the smaller size impactor was used.

Each failure, with one exception, showed the same failure mode as the static case shown in Fig. 15 and 16. The one exception occurred at 20 feet per second, and approached ballistic in nature. Figure 20 shows this failure with its almost complete penetration, and splaying of the delaminated layers on the back (non-impact) side.

Early in each test, damage was observed in the plates. This damage was localized in the immediate area of impact. When it started it was barely discernible using the liquid crystal technique, but as the tests progressed it became easier to see. After many impacts, the damaged area was delaminated, and this could be determined by careful tactile examinations. It did not appear to have any effect on the the ultimate failure energy. This "bruised" area was subjected to a microscopic examination. It was section 1A2 in Fig. 18 and is shown enlarged in subsequent figures.

TEST	SPEED (ft/sec)	NUMBER OF IMPACTS UNTIL FAILURE	PENETRATOR WEIGHT (lbs)	ULTIMATE IMPACT ENERGY (ft-lbs)
1A	10	18	1.7	2.64
2A	10	32	2.45	3.80
3C	10	13	2.5	3.88
4B	10	11	2.7	4.19
5D	10	6	3.0	4.66
AVERAGE	10	16	2.47	3.83
1B	15	7	1.0	3.49
2B	15	6	1.1	3.84
3B	15	5	1.1	3.84
5C	15	3	1.0	3.49
AVERAGE	15	5	1.05	3.67
1C	20	2	.55	3.42
2C	20	7	.75	4.66*
3A	20	2	.6	3.73
5A	20	3	.7	4.35
AVERAGE	20	3.5	.65	4.04

* BALLISTIC FAILURE MODE

Figure 19 - TABLE OF DYNAMIC TEST RESULTS

Figure 20 - BALLISTIC FAILURE MODE

VII. DISCUSSION OF RESULTS

There were three striking phenomena encountered during the course of the tests. The first was that the strain energy for failure in the static tests and the impact energy for failure in the dynamic tests were equal and constant. The second was the initial dynamic damage that occurred well before the ultimate failure. The third was the large deflections encountered.

As the tests and analyses progressed, the large deflections had an important influence on the correlation of experimental and theoretical results. The plates were .040 inches thick and static failure occurred at plate center deflections of approximately .35 inches. This means deflections were eight to nine times larger than the thickness of the plates.

An analysis was attempted to correlate the actual results with theoretical solutions. Five exact and finite element solutions were obtained for the static case and an intensive structural dynamic response analysis was attempted for the dynamic cases. These investigations were thwarted by inadequacies in the basic assumption of small deflections.

The plates all experienced a common failure mode for both the static and dynamic tests. Microscopy was utilized to examine this ultimate failure surface and mechanism. Further areas addressed with microscopy included: a pre-failure dynamic damage zone, or "bruise," that developed on each panel; a "yield" point that occurred during static

loading at approximately one half the ultimate load; and the fiber failure mechanism.

A. STRAIN RATE DEPENDENCE

As indicated in Fig. 14, in one large-penetrator test the specimen seemed to be significantly stiffer than the other plates, all of which showed quite similar load-deflection curves, regardless of penetrator size. The only parameter which differed in this "stiffer" test was the rate of loading, which was higher than that used in the other tests. No further qualitative analysis was performed, but the rate of loading was kept as low as possible. Further tests then yielded consistent, repeatable results.

B. FAILURE MODES

All failures, both static and dynamic, showed the same failure modes [Fig. 15, and 16]. There were only two exceptions. The first was during testing of the fixed plate with the smaller penetrator. This failure was illustrated in Fig. 17, and was a form of shear. Although the plate was stiffer than the simply supported plates, it responded in a similar manner until the "yield" point was reached. After that point, the penetrator virtually sheared through the plate. The second exception was one test at 20 feet per second. The failure mode approached ballistic in nature. Figure 20 illustrates the almost complete penetration, and the splayed lamina around the exit hole.

The choice of 20 feet per second as a limit for the dynamic tests was justified. Since one of the four tests

conducted experienced this failure mode, this speed range was in the transition from flexural failure mode to a ballistic failure mode.

The size of the plate was sufficient to keep the plate in the flexural failure, instead of shear failure, mode during static tests. All tests in the simply supported mode were flexural in nature.

1. Microscopic Examination of Ultimate Failure Area

Section 1A3 [Fig. 18] was cut and mounted for light microscope examination. Figure 21 shows the region outside of the gross delamination area typical of failure. This section appears relatively intact with very minor delamination. There are several small lamina fractures in the outer two layers running with the fiber directions in the matrix, and these minor cracks are associated with a slight delamination.

Figures 22, 23, and 24 show the lamina in the gross delamination region. These show extensive delamination, and numerous large cracks in the matrix, between fibers, penetrating entire laminas. Each delamination between laminas appears to have at least one crack penetrating the lamina directly above or below. Figure 24 illustrates this, with delaminations and associated fractures of the adjacent laminas.

Totally flexural failure damage should have been concentrated in the outermost layers where the largest stresses occurred. Figures 22, 23, and 24 all demonstrate a significant failure of the middle two layers in their

Figure 21 - LIGHT MICROSCOPE, FAILURE SURFACE EXAMINATION, SECTION 1A3, 100X

Figure 22 - LIGHT MICROSCOPE, FAILURE SURFACE EXAMINATION, SECTION 1A3, 100X

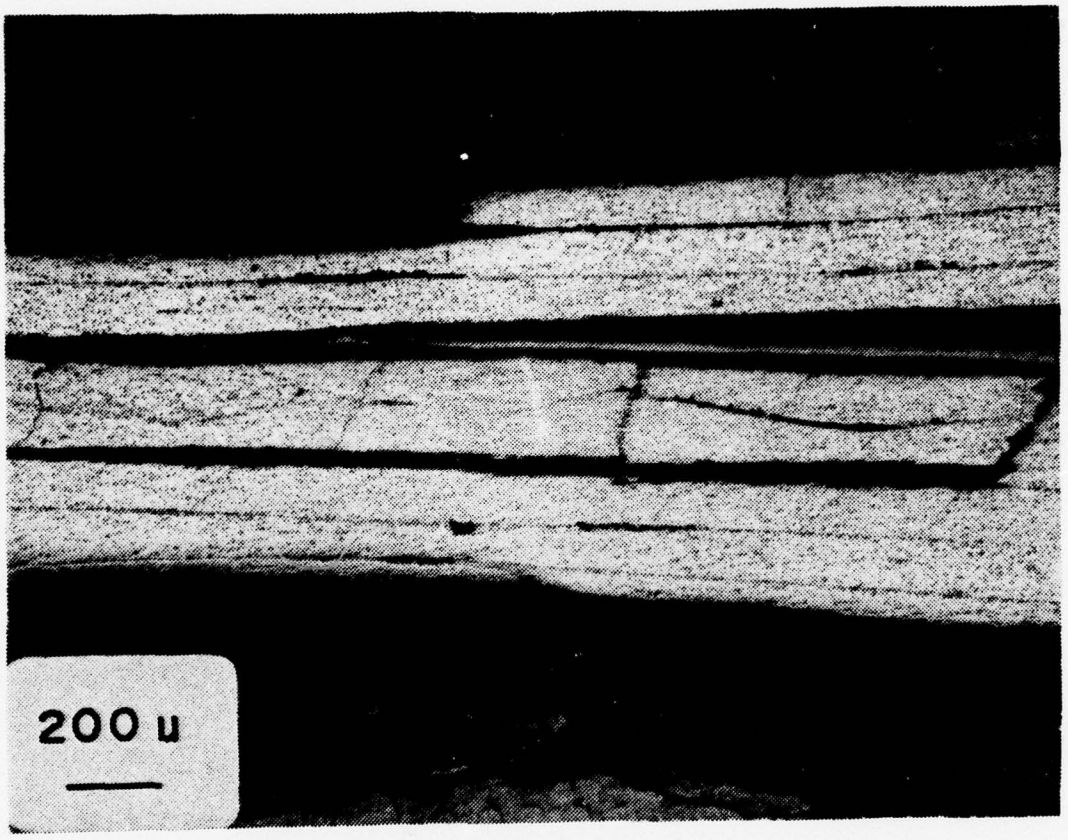

Figure 23 - LIGHT MICROSCOPE, FAILURE SURFACE EXAMINATION, SECTION 1A3, 50X

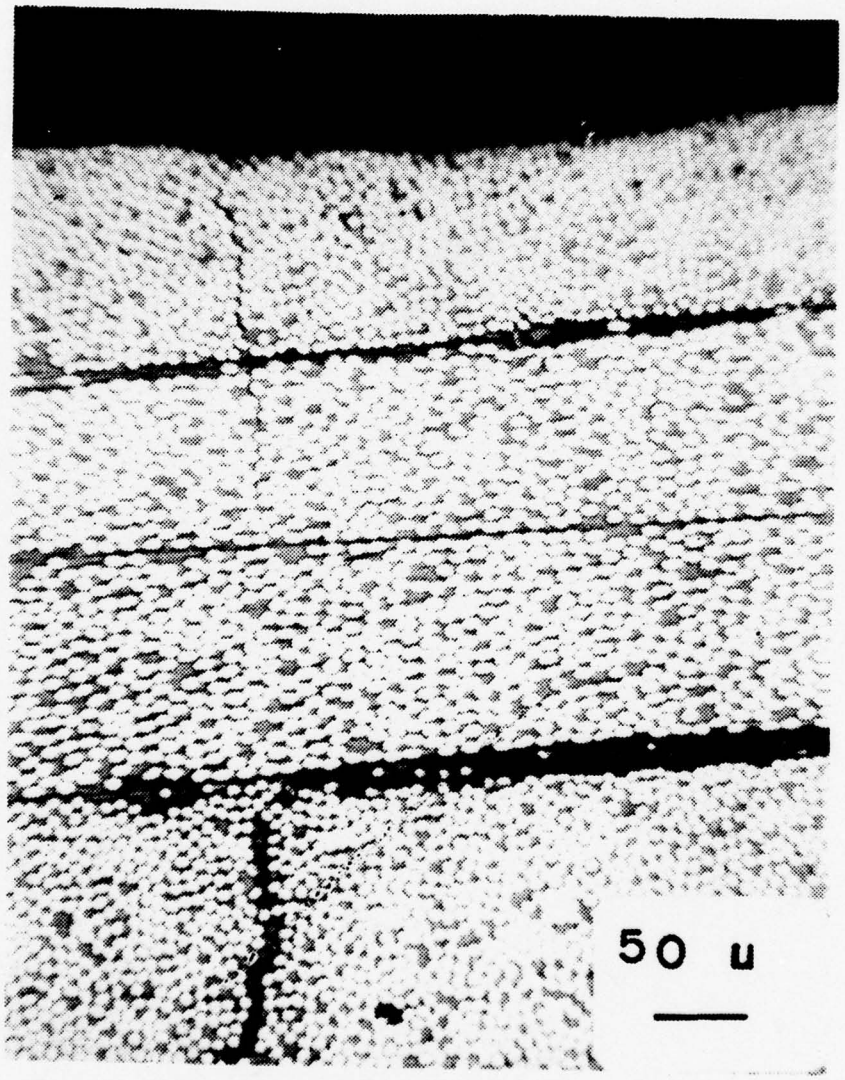

Figure 24 - LIGHT MICROSCOPE, FAILURE SURFACE EXAMINATION, SECTION 1A3, 200X

transverse direction. The assumption that the middle surface of the plate did not experience extension, therefore, is invalid. This would indicate that theoretical analysis based on small deflection theory is inappropriate.

In Figures 21, 22, and 24 the damage is most intense on only one side of the plate. The outer two layers on the side opposite the applied load appear almost intact. A quantitative examination of all failed plates showed an even distribution of damaged outer layers. Some plates showed gross lamina fracture in both outer layers. Other panels had damage on only the loaded side and vice-versa. Thus, the two intact layers are not considered significant.

A section was cut for the scanning electron microscope (SEM) evaluation as indicated in Fig. 18. Since this was an area of gross delamination, the top (or loaded side) two layers separated during sectioning. These layers were prepared for evaluation.

Figure 25 shows a typical fracture, or crack, in the epoxy matrix running through the outer layer. Figure 26 demonstrates a similar fracture, further illustrating the complete penetration of the lamina. The entire outer layer, a zero degree layer, was extensively cracked. Figures 27, 28, 29, and 30 show typical fractures in the first 45 degree layer.

Figures 27, 29, and 30 have remnants of the third inner layer (45 degrees) which are evident as epoxy and some fiber fragments running at right angles to the original layer. This was typical of all the gross delamination surfaces.

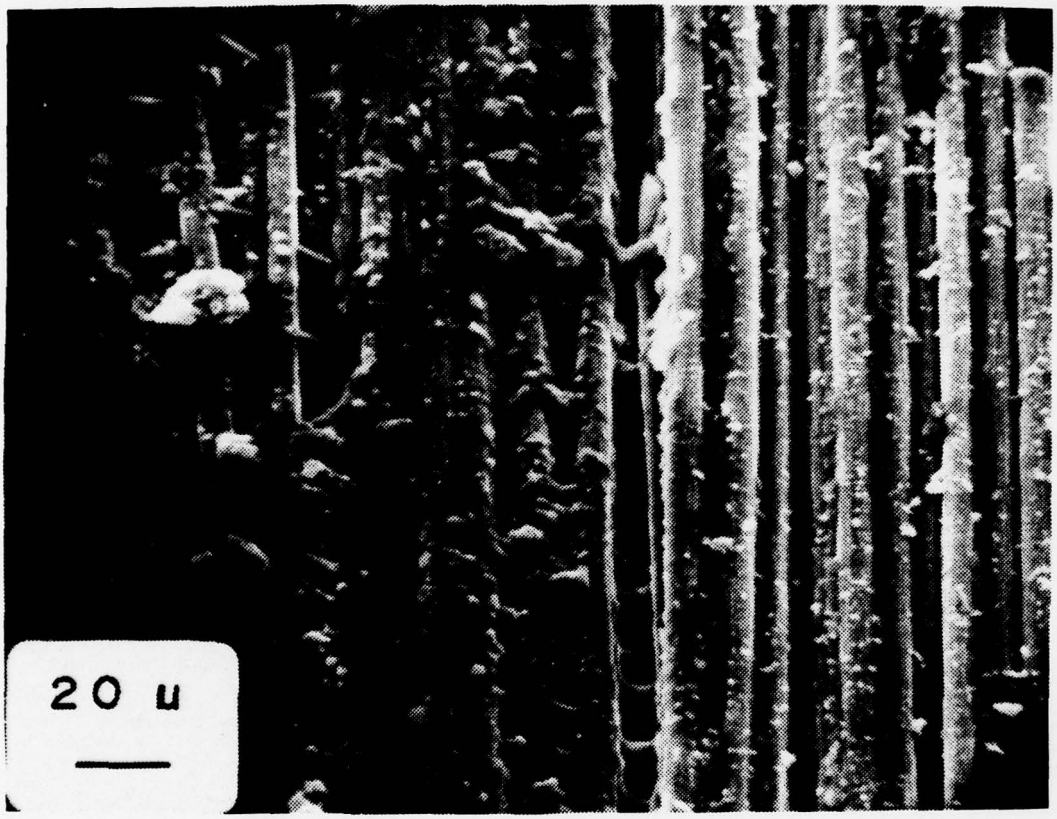

Figure 25 - SEM, TYPICAL FRACTURE IN OUTER LAYER, 520X

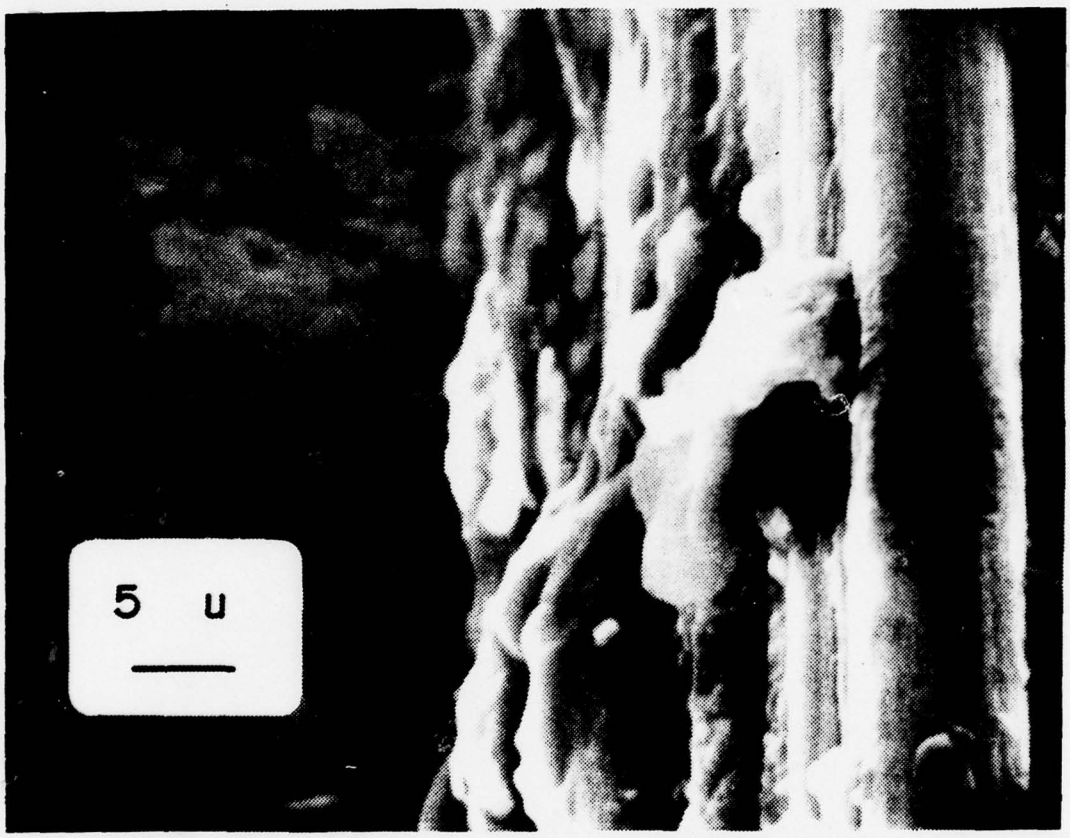

Figure 26 - SEM, TYPICAL FRACTURE IN OUTER LAYER, 2200X

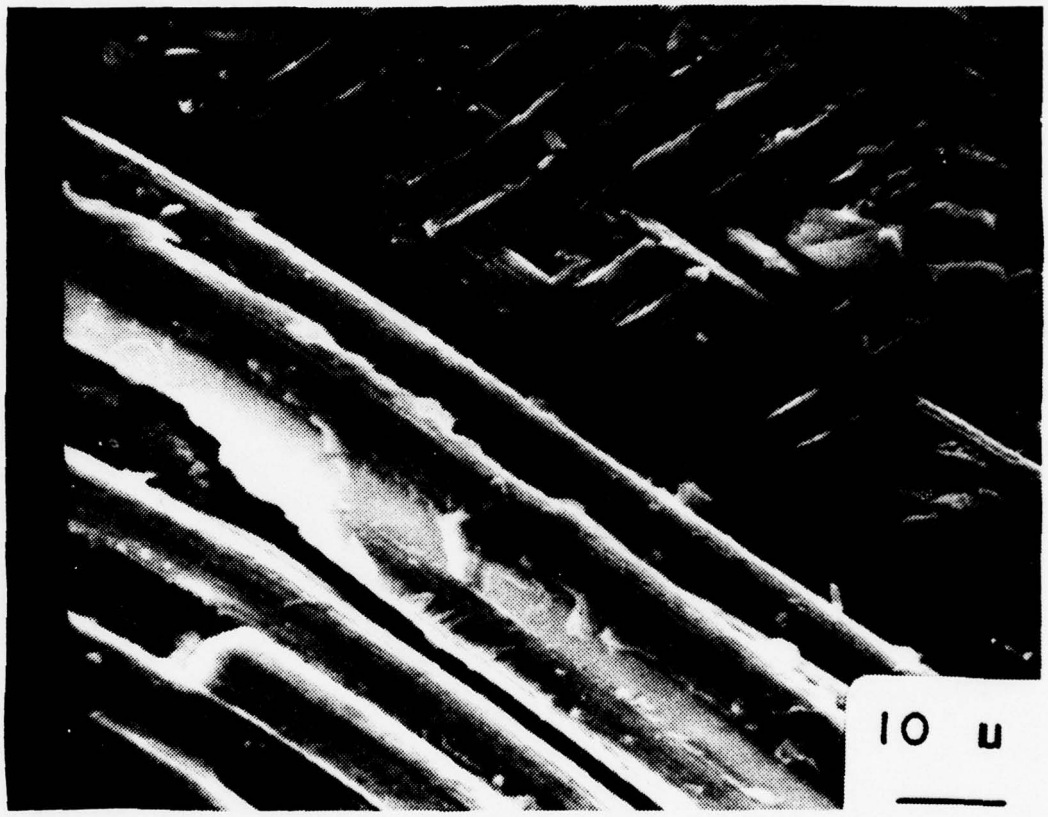

Figure 27 - SEM, TYPICAL FRACTURE IN SECOND LAYER, 1200X

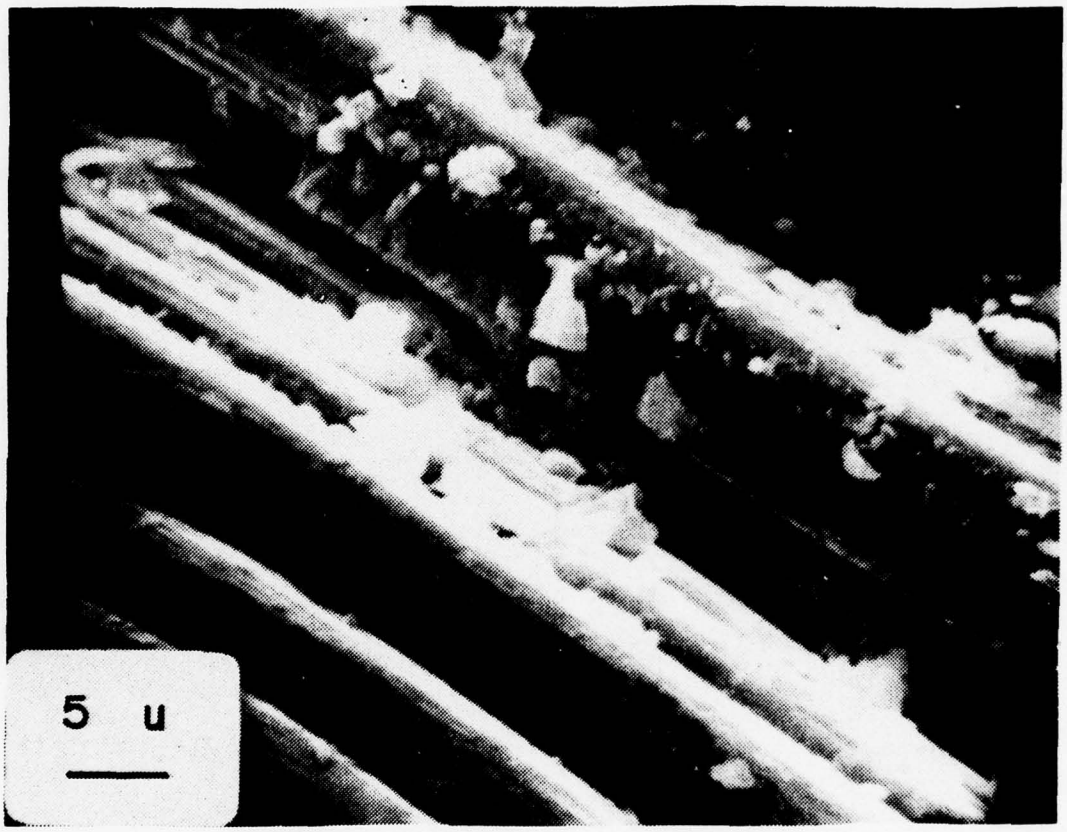

Figure 28 - SEM, TYPICAL FRACTURE IN SECOND LAYER, 2200X

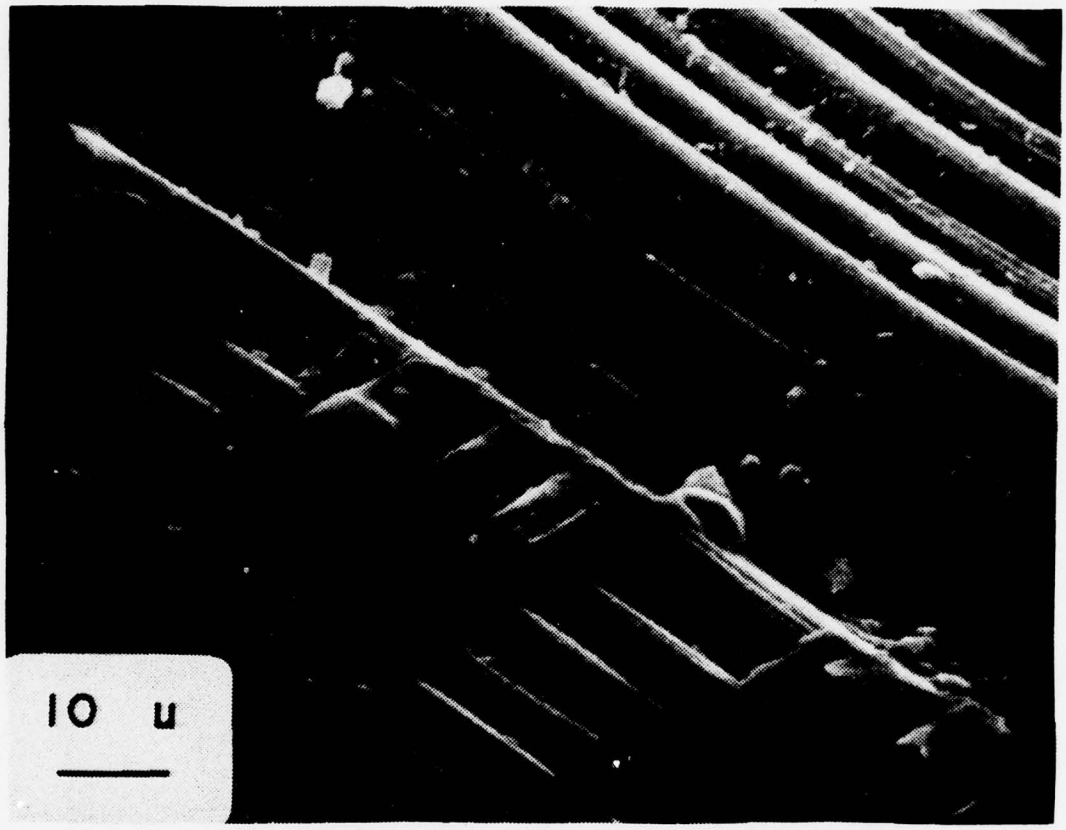

Figure 29 - SEM, TYPICAL FRACTURE IN SECOND LAYER, 1200X

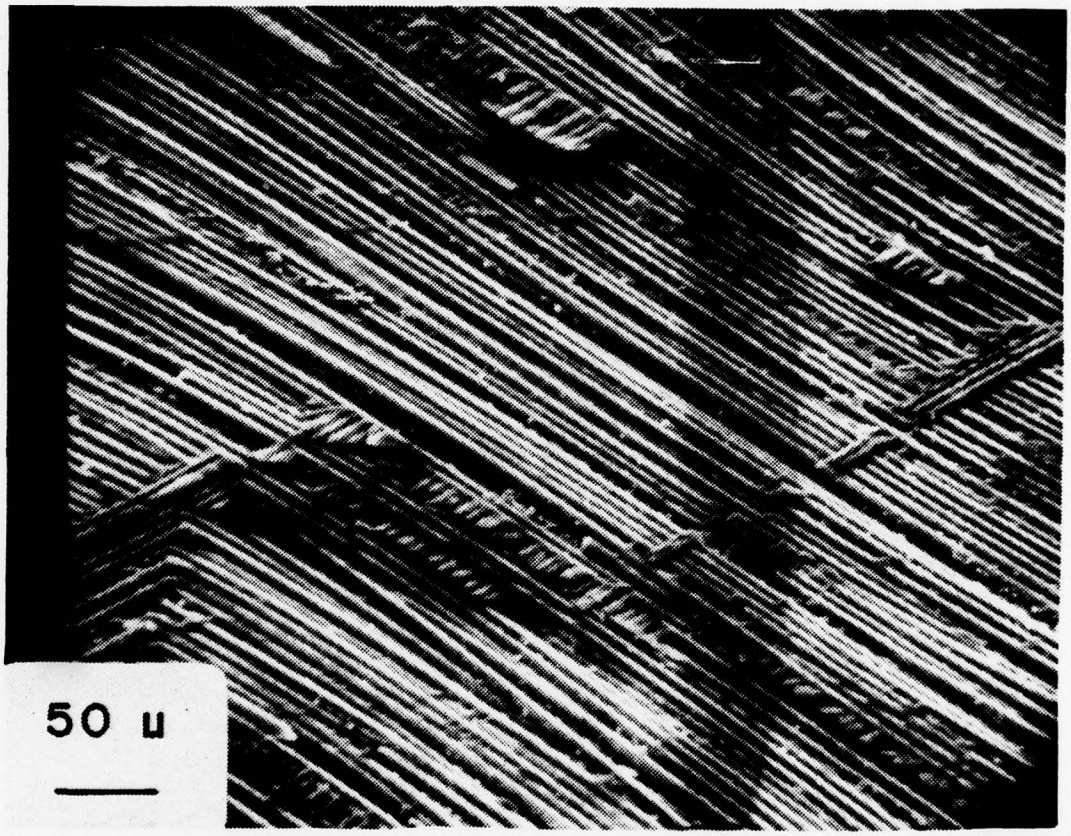

Figure 30 - SEM, TYPICAL FRACTURE IN SECOND LAYER, 220X

Of particular interest is the continuity of the fibers in the layers. All inter-laminar failures occurred at the epoxy-fiber joints with no discernible fiber breakage. A quantitative analysis, presented in Fig. 31, indicates that slightly over ten percent of the inner lamina epoxy-fiber joints have broken. These failures are long, parallel to the fibers, continuous, and appear to penetrate completely. This would indicate an inability to carry any load in the transverse direction while still maintaining strength in the fiber direction. This would be consistent with the low transverse, but very high longitudinal, strength and failure characteristics. The transfer of this transverse load to the next lamina would cause large inter-laminar shear forces, and this could account for the gross delaminations. The observation that all delaminations appear to have an associated matrix fracture, or crack, further supports this theory.

	FIGURE 29	FIGURE 30
TOTAL LENGTH OF FRACTURES	.01 cm	.3014 cm
AREA OF PHOTOGRAPH	7.39×10^{-5} cm^2	.0022 cm^2
LENGTH OF FRACTURE divided by TOTAL AREA	135 cm/cm^2	137 cm/cm^2
AVERAGE FIBER LENGTH	7.1 cm	7.2 cm
APPROXIMATE NUMBER OF FIBER/EPOXY JOINTS	16	86
LENGTH AVAILABLE TO FORM FRACTURES	113.6 cm	612 cm
PERCENTAGE OF FIBER/EPOXY JOINTS BROKEN	10.6 %	10.7 %

Figure 31 - QUANTITATIVE ANALYSIS OF FAILURE OF FIBER-EPOXY JOINTS

2. Microscopic Examination of Static "Yield" Point

During static loading of the plates, there was a pronounced "yield" point at approximately half the ultimate load. At this point the panel would experience a decreased load with no increase in displacement, accompanied by loud cracking noises. Figure 14 gives plots of these points. A plate was loaded just past this "yield" point, and then sectioned (5B) as shown in Fig. 13. Using the light microscope, Fig. 32 shows an area where all eight lamina are delaminated. In Fig. 33 there are just a few delaminations, but both pictures show extensive damage to the underside (side opposite the load) zero degree layer.

Figures 34, 35, and 36 all show the same damage to the bottom layer along with assorted other delaminations and cracks. Figures 34 and 35 have matrix fractures associated with delaminations. In the microphotographs, the damaged outer layer was probably accentuated by the reaction of the plastic mounting material with the epoxy, as previously described.

Although there were other varied types of damage, the major fracture mechanism was the failure of the zero degree lamina on the side opposite the load. It is conjectured that the "yield" point encountered is the failure of the outer layer in the transverse direction and the shifting of this load to the inner laminas. Due to the geometry of the lay-up and the strength characteristics, the next two 45-degree laminas could more efficiently carry the load transverse to the zero-degree layer.

The useful, or safe working, load of the plate would be limited by this "yield" point.

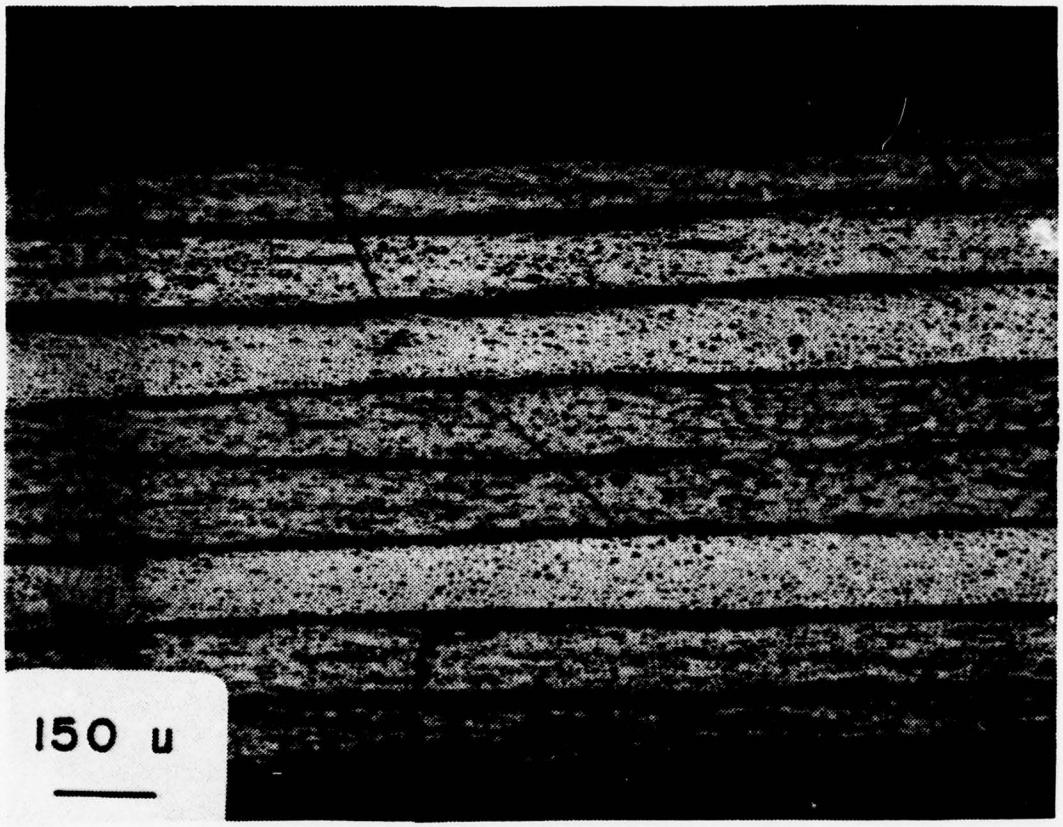

Figure 32 - LIGHT MICROSCOPE, "YIELD" POINT EXAMINATION, SECTION 5B, 75X

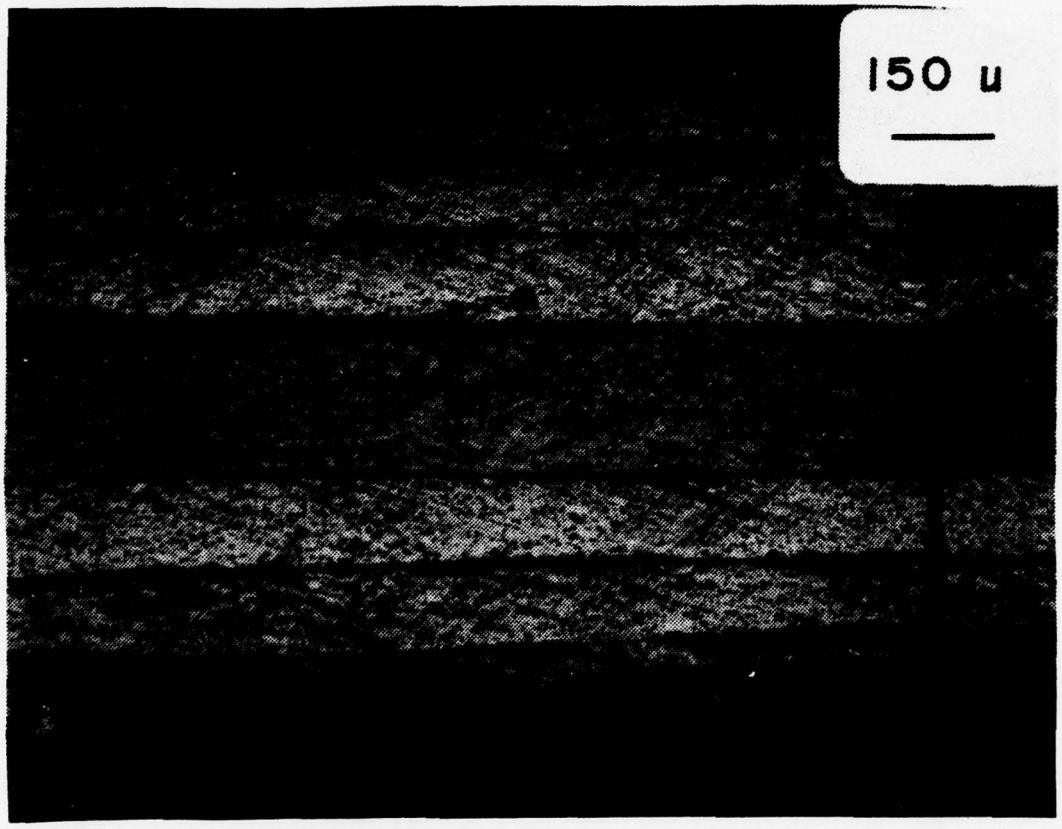

Figure 33 - LIGHT MICROSCOPE, "YIELD" POINT EXAMINATION, SECTION 5B, 75X

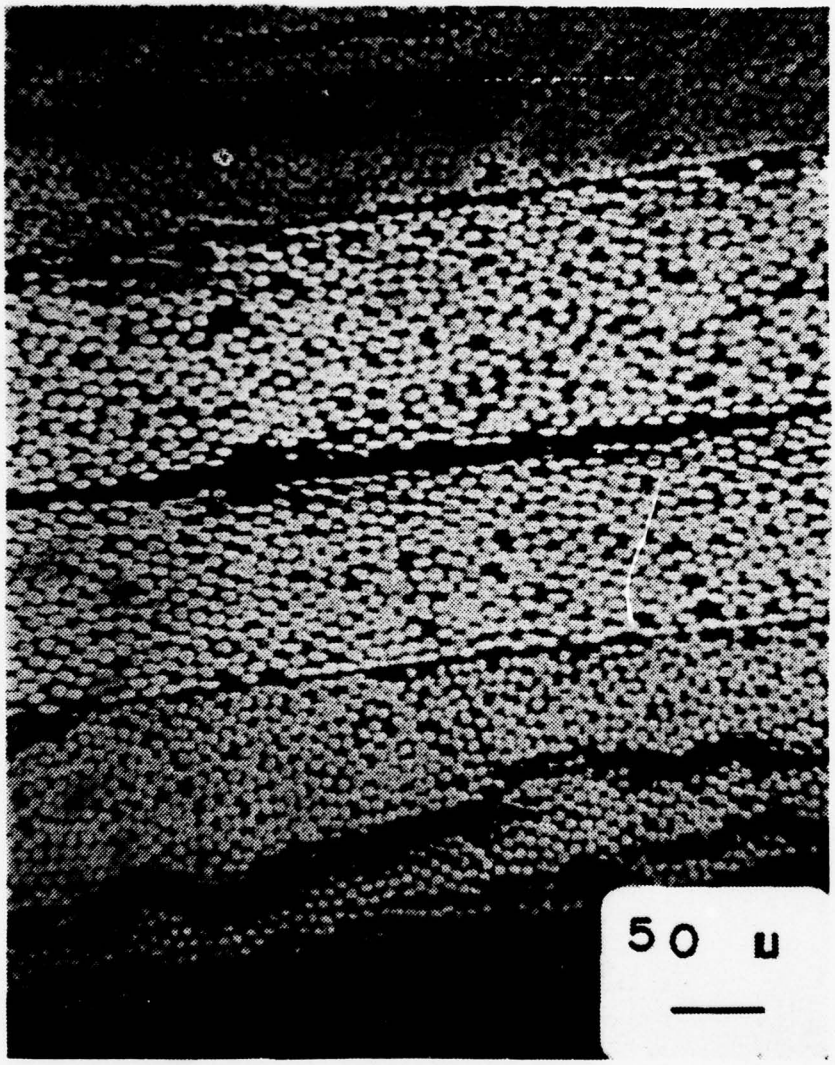

Figure 34 - LIGHT MICROSCOPE, "YIELD" POINT EXAMINATION, SECTION 5B, 200X

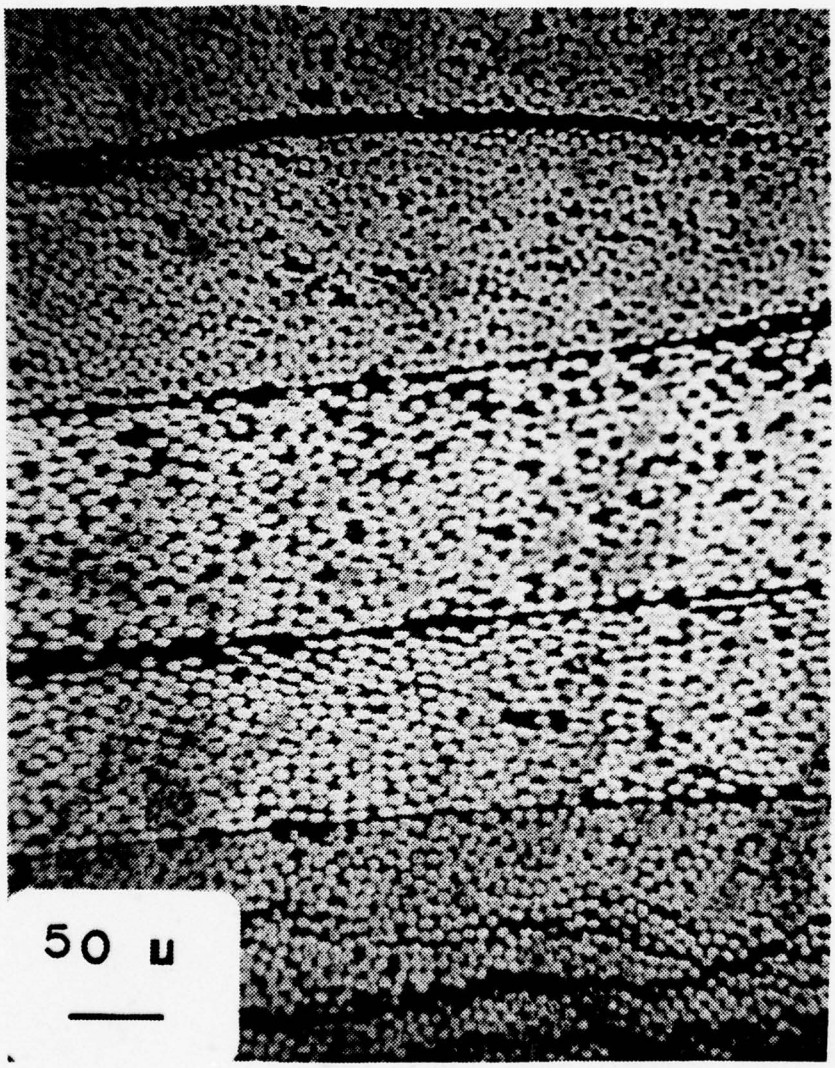

Figure 35 - LIGHT MICROSCOPE, "YIELD" POINT EXAMINATION, SECTION 5B, 200X

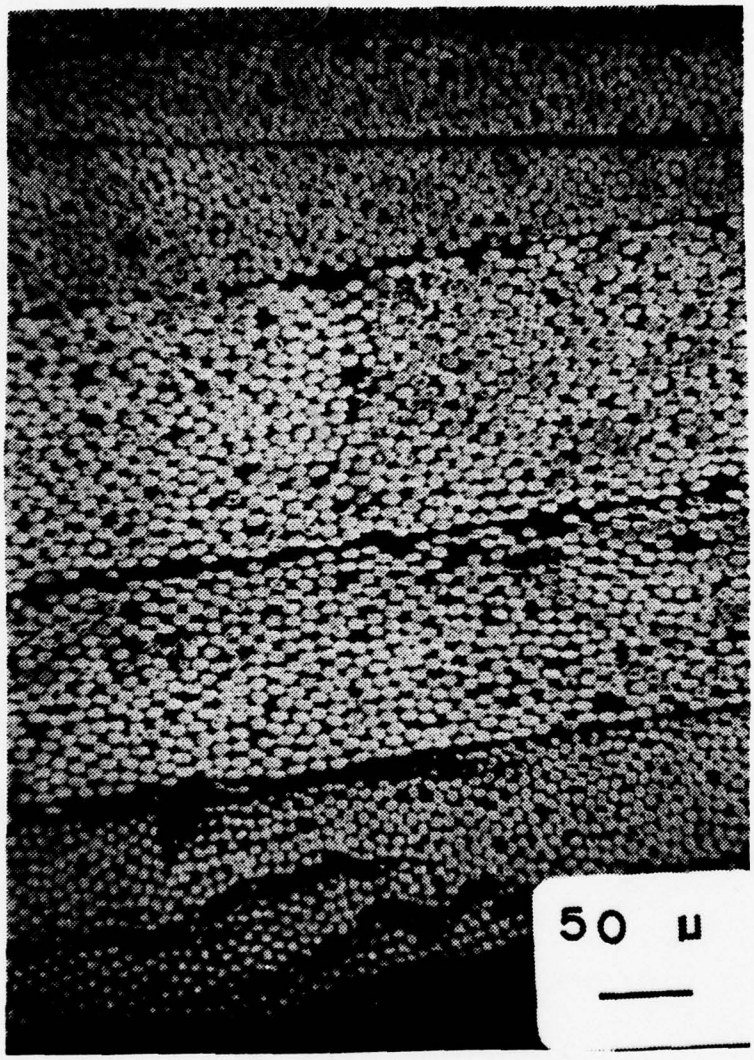

Figure 36 - LIGHT MICROSCOPE, "YIELD" POINT EXAMINATION, SECTION 5B, 200X

3. Microscopic Examination of Initial Dynamic Damage Zone

Early in the impact loading history, a "bruise" was noted in the immediate impact area. This abnormality could first be detected using the liquid crystal inspection method. As each test progressed, the "bruise" could be detected by carefully sighting across the face of the panel where it appeared as a slight bulge. This damaged area never grew larger than the immediate area of impact.

To examine this phenomenon further, a section (1A2) was cut from a panel as shown in Fig. 18. Figure 37 is in an area just outside the "bruise" and shows little damage. Figure 38 is in the edge of the pre-failure damage area, and has all plies, with the exception of the middle two, starting to delaminate. Figure 39 is well into the impact area and delamination is extensive.

The "bruise" delamination and the typical failure differ. In the "bruise" area, more lamina are involved extensively without as many associated matrix failures in adjacent lamina. There are also no failures of the inner two laminas in the transverse direction.

This damage mechanism is theorized to be a form of spalling caused by the intensive compressive stress wave traveling through the thickness of the material on impact; Ref. 10 applies.

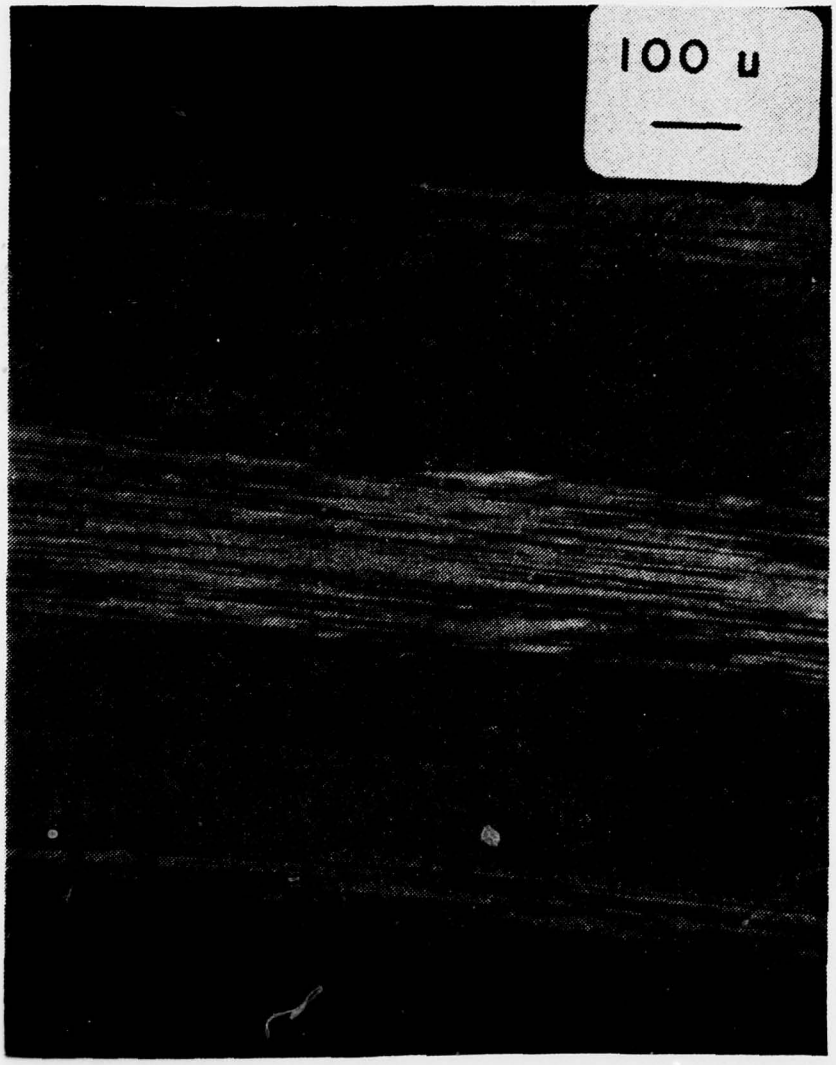

Figure 37 - LIGHT MICROSCOPE, LOCALIZED DYNAMIC DAMAGE, SECTION 1A2, 100X

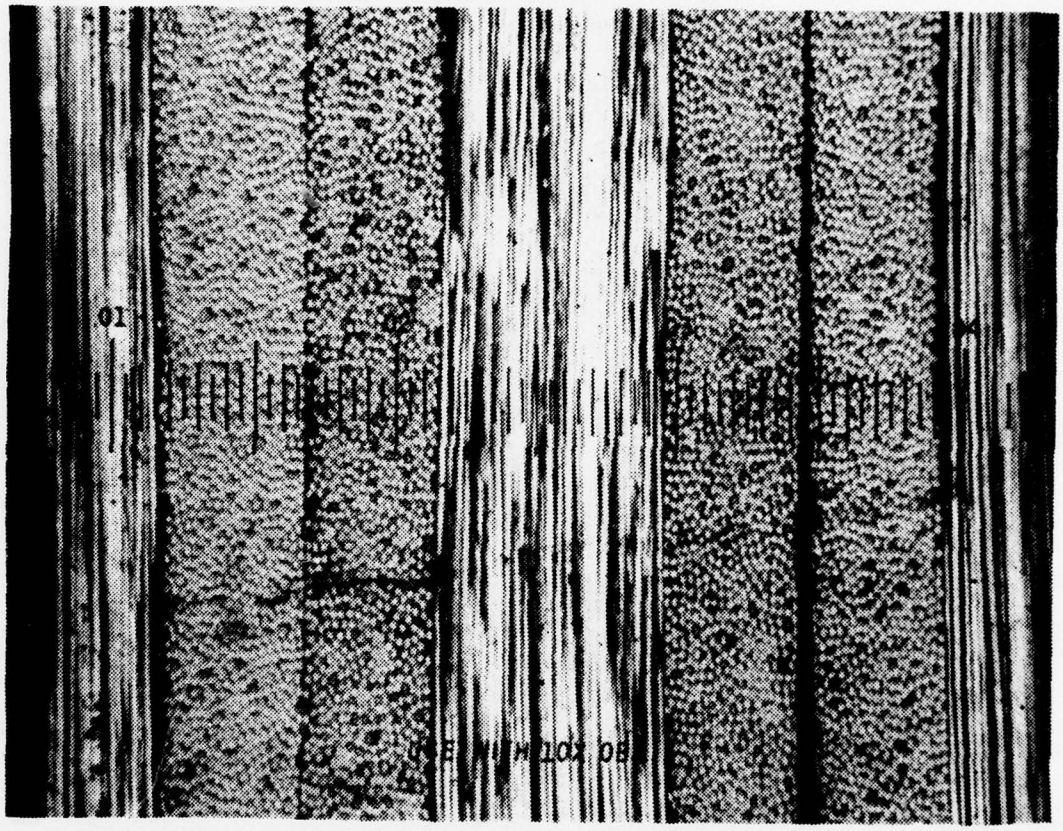

Figure 38 - LIGHT MICROSCOPE, LOCALIZED DYNAMIC DAMAGE, SECTION 1A2

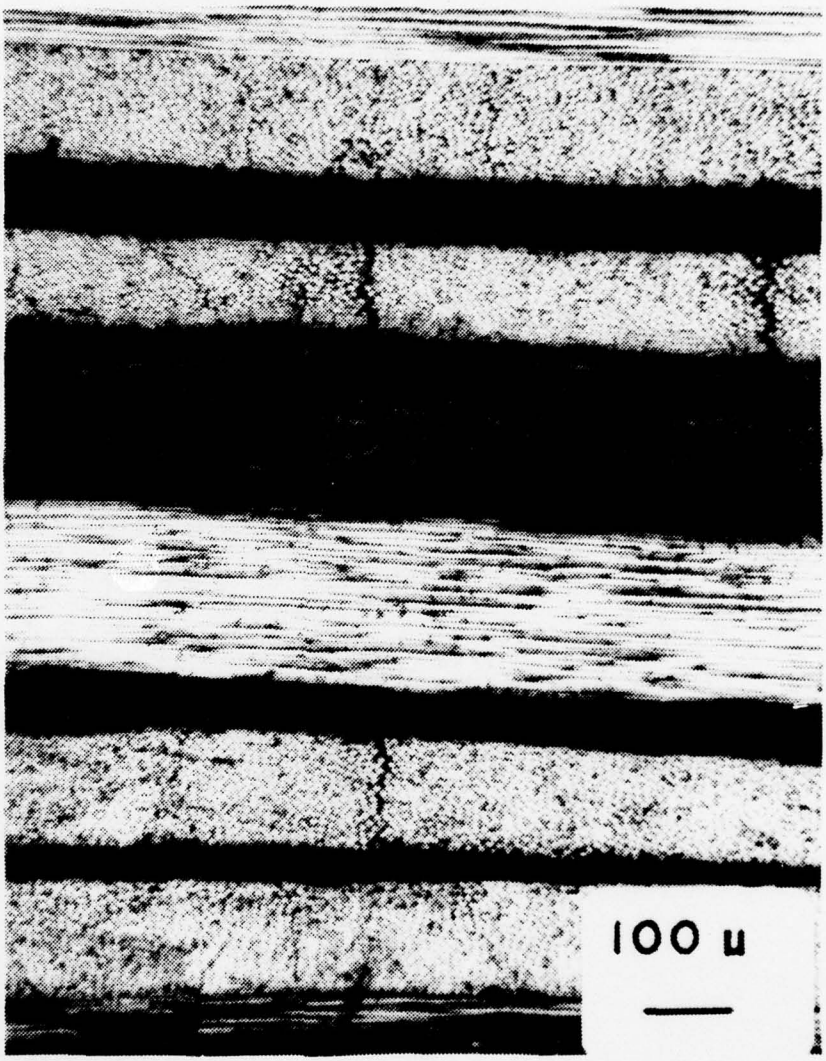

Figure 39 - LIGHT MICROSCOPE, LOCALIZED DYNAMIC DAMAGE, SECTION 1A2, 100X

4. Microscopic Examination of Fiber Failures

Very few fiber failures were found, and the cause of those failures was hard to determine.

Figure 40 shows a single broken fiber in the 45 degree layer of the Scanning Electron Microscope sample. Figure 41 shows a bundle of broken fibers in the zero degree outer layer of the same specimen.

The broken fibers in these pictures show 45 degree fracture surfaces. This would be indicative of shear fracture under high strain rates according to Coangelo and Heiser [Ref. 11]. They could also just be the ends of the fibers as manufactured.

Because of the rarity of broken fibers and the fact that fibers are not normally continuous in a lamina, no significance was assigned to these fiber fractures.

It appears the lack of strength of the laminas in the transverse direction was the significant factor in failure of these plates. Adding 90 degree laminas might have provided a large increase in impact resistance and static strength.

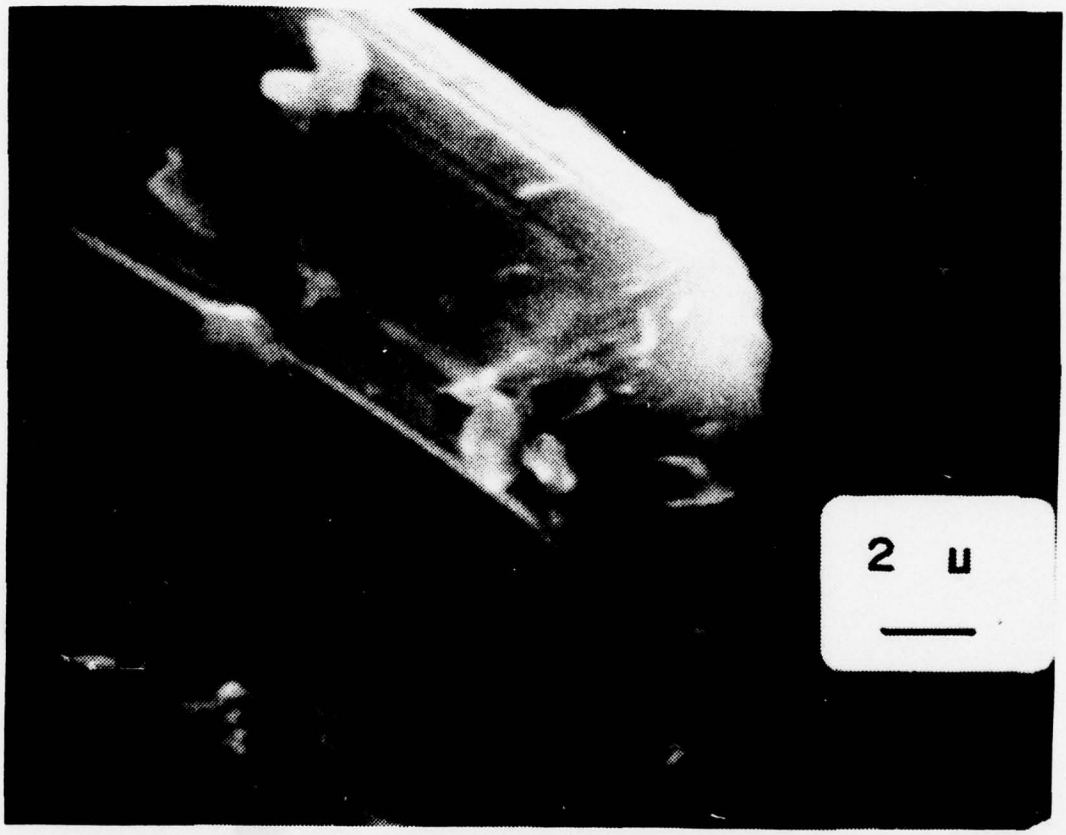

Figure 40 - SEM, A BROKEN FIBER, 5200X

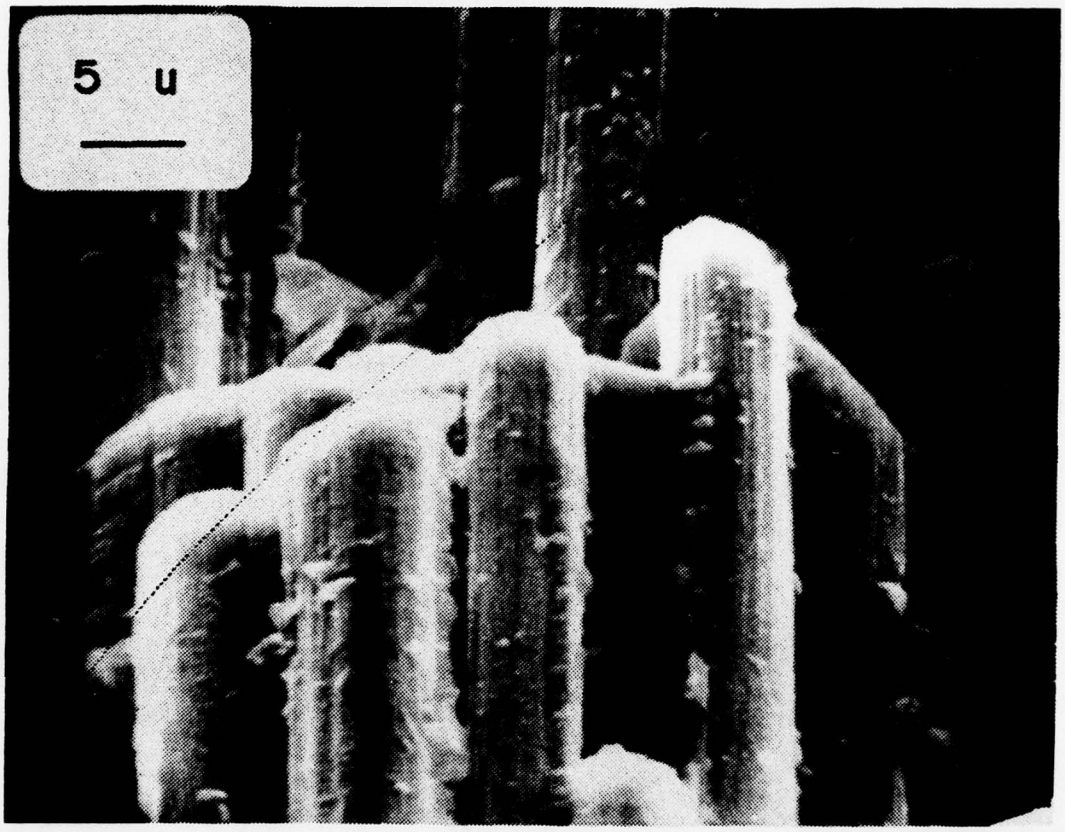

Figure 41 - SEM, A BUNDLE OF BROKEN FIBERS, 2200X

C. ENERGY REQUIRED FOR FAILURE

Figure 42 is a plot of the energy required for ultimate failure for both dynamic and static cases. Only simply supported plates, using the small penetrator, were plotted. A least-squares fit of first and second order were plotted, and, within experimental accuracy, the energy for failure in both static and dynamic cases was constant.

Since a constant impact energy mechanism was manifest and this energy equalled the static strain energy to failure, the correct dynamic model seems to be a one degree-of-freedom lumped parameter spring mass system [Ref. 9]. The general, continuous, structural dynamic response model was not indicated. However, an extensive series of dynamic response studies was performed using the dynamic response section of SAP IV [Ref. 5]. The parameters of impact duration, impact shape, number of natural modes utilized, and constitutive properties were all varied. In all results the experimental values showed the actual plate as being significantly stiffer than the model, and no correlation between the experimental results and the finite element dynamic structural response analysis could be obtained.

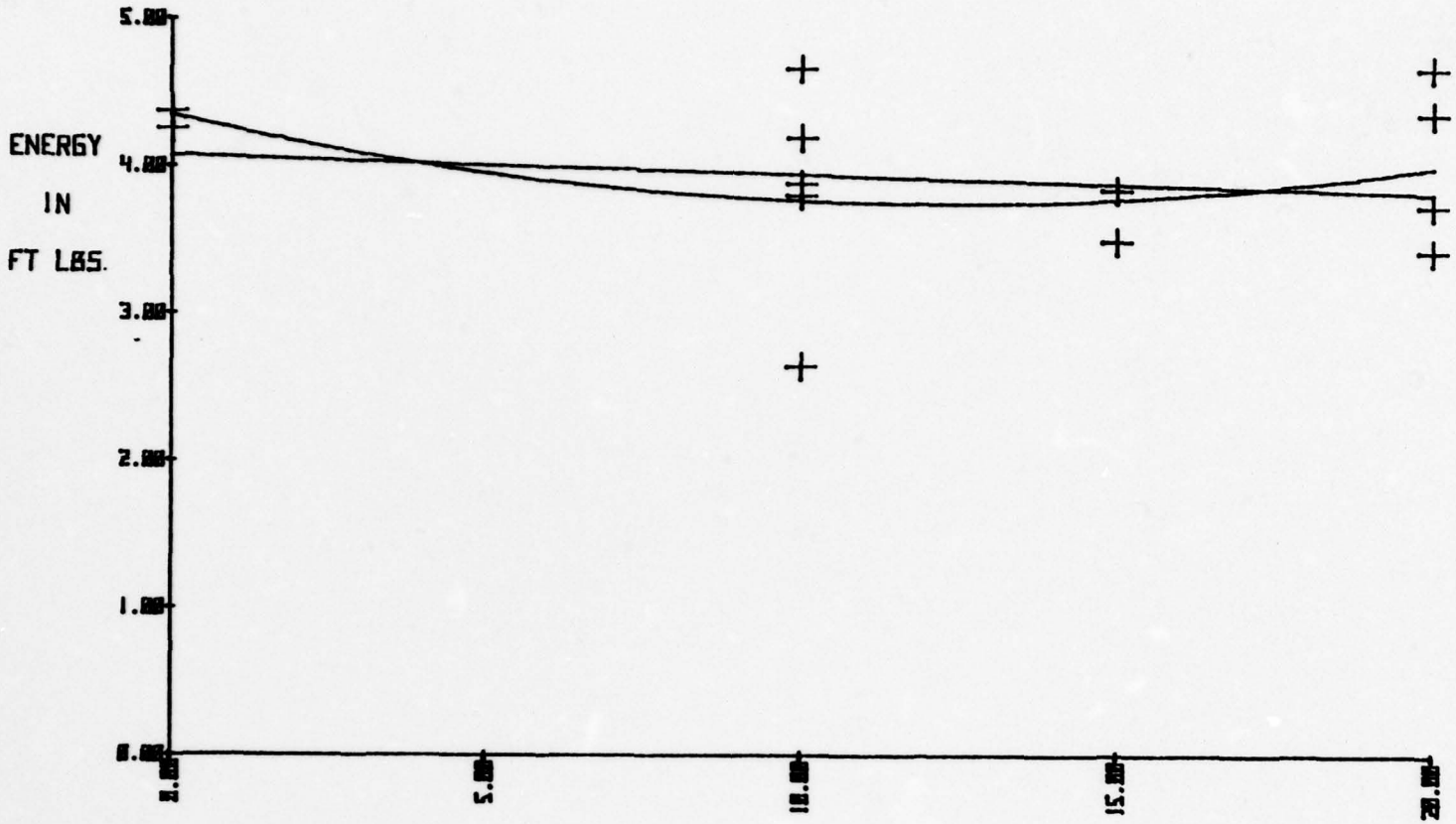

Figure 42 - IMPACT ENERGY REQUIRED FOR FAILURE

D. STATIC SOLUTIONS

With a constant impact energy failure, a static solution to the plate problem would also provide the dynamic solution. Figure 43 is a plot of several different solutions and the average experimental results.

The exact solution of Timoshenko and Woinowsky-Krieger [Ref. 7] for an orthotropic plate were computed and plotted. The design manual's [Ref. 2] exact solution was also plotted using both sets of developed constitutive properties.

The finite element model was used for the fixed edge solution, and the simply supported solution using the small penetrator. It was also used for the simply supported solution using the large penetrator. The large penetrator was simulated using the experimentally obtained displacements. A drawing was made of the displacements with the penetrator overlaid. The load was assumed to be a pressure distribution in the same shape and proportion to the contact area of the penetrator on the displaced plate.

As can be seen from Fig. 43, the theoretical results agreed well among themselves. The exact and finite element solution for a concentrated load were within a percentage point; however, the theoretical and experimental results were in significant disagreement.

From the microscopic analysis, the static theoretical analysis, and the dynamic theoretical analysis it was determined that small deflection theory was unusable. These plates, due to their small thickness and relative flexability, were more appropriately considered in large

deflection theory.

Chi-Teh Wang [Ref. 12] has solved the static problem for a large deflection, simply supported, uniformly loaded plate. Although not directly applicable to the problem considered here, his results show the same general form for a uniformly loaded plate as these experimental results for a concentrated load plate.

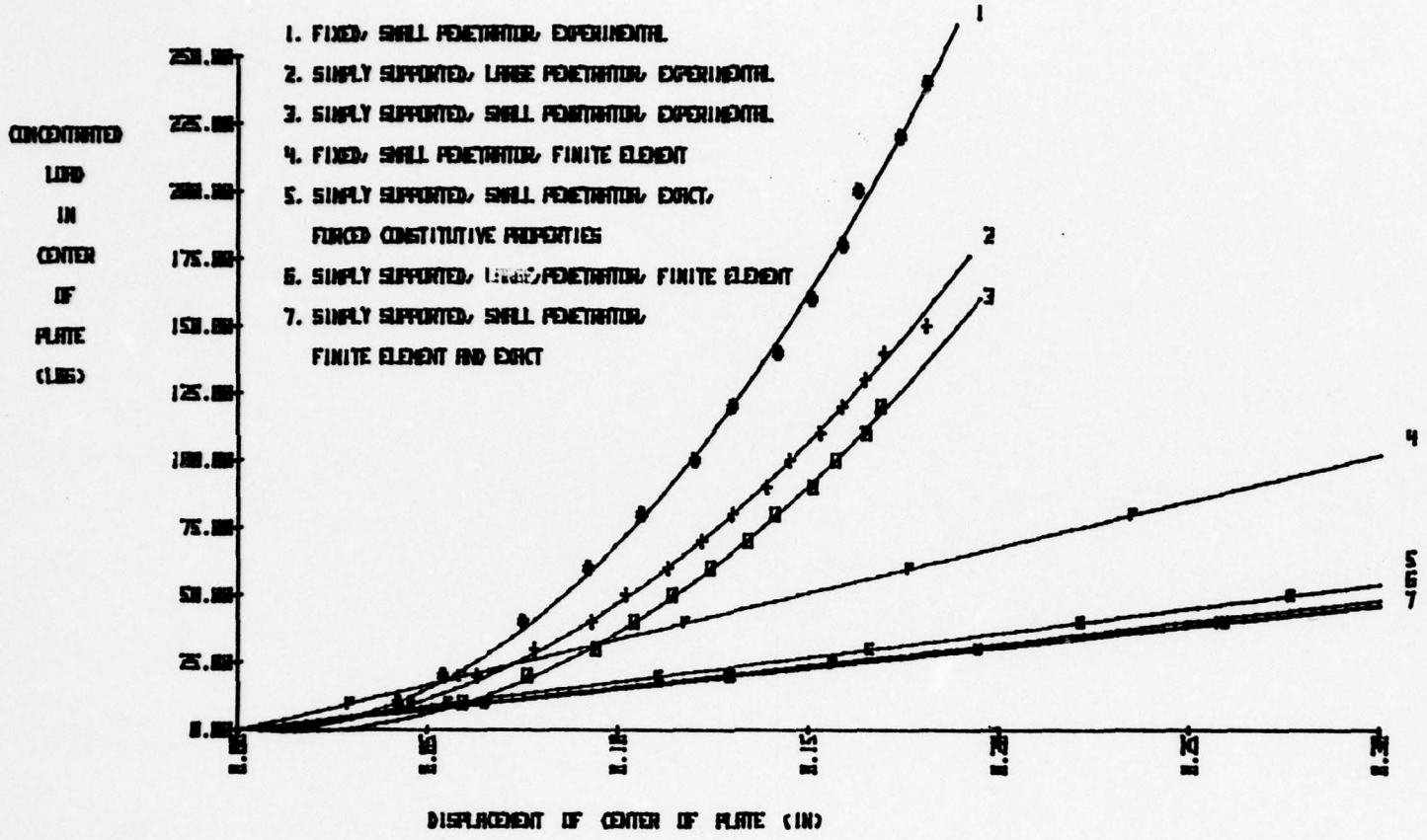

Figure 43 - EXACT, FINITE ELEMENT, AND EXPERIMENTAL RESULTS OF THE STATIC TESTS

VIII. CONCLUSIONS

A. The dynamic and static failure modes for simply supported graphite-epoxy plates under either central concentrated load or low-energy impact are the same.

B. Between zero and twenty feet per second large deflection failures of graphite-epoxy, simply supported plates occurred at a constant energy.

C. There was a "yield point" where damage occurred in static loading.

E. There was localized stress wave damage in the immediate, dynamic contact area.

F. Linear, small-deflection theory is not applicable to thin graphite-epoxy plates loaded to failure.

IX. RECOMMENDATIONS

An exact, large deflection solution should be developed to analyze thin plate responses to concentrated loads. Once this solution is in hand, a good approximation can be made for low energy, dynamic damage thresholds using energy methods. This information can then be used for both design and operational maintenance.

APPENDIX A

CONSTITUTIVE PROPERTIES COMPUTER PROGRAM

```
10 DIM Q[3,3],R[3,3],S[3,3],C[3,3],D[3,3],H[9],E[8]
20 DIM A[3,3],G[3,3],F[3,3]
30 E1=2.2E+07
40 E2=1.6E+06
50 G1=6E+05
60 V1=0.2
70 V2=0.014
80 Q[1,1]=E1/(1-V1*V2)
90 Q[1,2]=V1*E2/(1-V1*V2)
100 Q[2,2]=E2/(1-V1*V2)
110 Q[3,3]=G1
120 Q[2,1]=Q[1,2]
130 Q[3,1]=0
140 Q[3,2]=0
150 Q[1,3]=0
160 Q[2,3]=0
170 PRINT "ZERO PLY MATRIX"
180 MAT PRINT Q
190 DEG
200 T1=45
210 FOR I=1 TO 2
220 T3=(COS(T1))↑4
230 T4=(SIN(T1))↑2*(COS(T1))↑2
240 T5=(SIN(T1))↑4
250 T6=(SIN(T1))↑4+(COS(T1))↑4
260 T7=SIN(T1)*(COS(T1))↑3
270 T8=(SIN(T1))↑3*COS(T1)
280 R[1,1]=Q[1,1]*T3+2*(Q[1,2]+2*Q[3,3])*T4+Q[2,2]*T5
290 R[1,2]=(Q[1,1]+Q[2,2]-4*Q[3,3])*T4+Q[1,2]*T6
300 R[2,1]=R[1,2]
310 L9=Q[1,2]-Q[2,2]+2*Q[3,3]
320 R[1,3]=(Q[1,1]-Q[1,2]-2*Q[3,3])*T7-L9*T8
330 R[2,2]=Q[1,1]*T5+2*(Q[1,2]-2*Q[3,3])*T4+Q[2,2]*T3
340 R[2,3]=(Q[1,1]-Q[1,2]-2*Q[3,3])*T8+L9*T7
350 R[3,1]=R[1,3]
360 R[3,2]=R[2,3]
370 R[3,3]=(Q[1,1]+Q[2,2]-2*Q[1,2]-2*Q[3,3])*T4+Q[3,3]*T6
380 T1=T1*(-1)
390 PRINT "    45 DEGREE PLY"
400 MAT PRINT R
410 IF I=2 THEN 480
420 FOR J=1 TO 3
430 FOR K=1 TO 3
440 S[J,K]=R[J,K]
450 NEXT K
460 NEXT J
470 NEXT I
```

AD-A035 890 NAVAL POSTGRADUATE SCHOOL MONTEREY CALIF F/G 11/4
LOW ENERGY IMPACT LOADING OF GRAPHITE-EPOXY PLATES.(U)
DEC 76 R L FERRIS

UNCLASSIFIED NL

2 OF 2
ADA035890

END
DATE FILMED
3-77

```
480 H1=0.04
490 H[1]=-0.015
500 H[2]=-0.01
510 H[3]=-0.005
520 H[4]=0
530 H[5]=0.005
540 H[6]=0.01
550 H[7]=0.015
560 H[8]=0.02
570 FOR I=1 TO 3
580 FOR J=1 TO 3
590 B9=0.005
600 E[1]=Q[I,J]*B9
610 E[2]=R[I,J]*B9
620 E[3]=S[I,J]*B9
630 E[4]=Q[I,J]*B9
640 E[5]=Q[I,J]*B9
650 E[6]=S[I,J]*B9
660 E[7]=R[I,J]*B9
670 E[8]=Q[I,J]*B9
680 F[I,J]=(E[1]+E[2]+E[3]+E[4]+E[5]+E[6]+E[7]+E[8])
690 NEXT J
700 NEXT I
710 PRINT "  A MATRIX"
720 MAT PRINT F
730 FOR I=1 TO 3
740 FOR J=1 TO 3
750 E[1]=Q[I,J]*(H[1]↑3-(-0.02)↑3)
760 E[2]=R[I,J]*(H[2]↑3-H[1]↑3)
770 E[3]=S[I,J]*(H[3]↑3-H[2]↑3)
780 E[4]=Q[I,J]*(H[4]↑3-H[3]↑3)
790 E[5]=Q[I,J]*(H[5]↑3-H[4]↑3)
800 E[6]=S[I,J]*(H[6]↑3-H[5]↑3)
810 E[7]=R[I,J]*(H[7]↑3-H[6]↑3)
820 E[8]=Q[I,J]*(H[8]↑3-H[7]↑3)
830 G[I,J]=(E[1]+E[2]+E[3]+E[4]+E[5]+E[6]+E[7]+E[8])/3
840 H[I,J]=G[I,J]*(H↑3)/12
850 NEXT J
860 NEXT I
870 PRINT "     D              MATRIX"
880 MAT PRINT G
890 E1=(F[1,1]*F[2,2]-F[1,2]↑2)/(H1*F[2,2])
900 E2=E1*F[2,2]/F[1,1]
910 E3=F[3,3]/H1
920 V1=F[1,2]/F[1,1]
930 V2=F[1,2]/F[2,2]
940 PRINT "       EXX          EYY.         EXY"
950 PRINT E1;E2;E3
960 PRINT "     V12          V21"
970 PRINT V1;V2
980 PRINT LIN2
990 MAT A=ZER
1000 Q9=(1-V1*V2)
1010 A[1,1]=E1/Q9
```

```
1020 A[1,2]=V1*E1/09
1030 A[2,1]=A[1,2]
1040 A[2,2]=E2/09
1050 A[3,3]=E3
1060 PRINT " C MATRIX"
1070 MAT PRINT A
1080 STOP
1090 END
```

AN EXAMPLE OUTPUT

ZERO PLY MATRIX

22061772.96	320398.5158	0
320398.5158	1604492.579	0
0	0.	600000

45 DEGREE PLY

6677015.644	5477015.644	5114320.096
5477015.644	6677015.644	5114320.096
5114320.096	5114320.096	5756117.128

45 DEGREE PLY

6677015.644	5477015.644	-5114320.096
5477015.644	6677015.644	-5114320.096
-5114320.096	-5114320.096	5756117.128

A MATRIX

574775.7722	115958.2632	0
115958.2632	165630.1645	0
0	0	127122.3426

D MATRIX

84.32914828	12.88304586	-5.114320096
12.88304586	19.54776040	-5.114320096
-5.114320096	-5.114320095	14.37158711

EXX	EYY	EXY
12339823.86	3555903.284	3178058.564

V12	V21
0.201745252	0.700103653

C MATRIX

14369894.3	2898957.060	0
2898957.060	4148754.112	0
0	0	3178058.564

APPENDIX B

FAILURE EVALUATION COMPUTER PROGRAM

```
10 DIM Q[3,3],R[3,3],S[3,3],C[3,3],D[3,3],H[9],E[3]
20 DIM A[3,3],O[3],P[3],T[3],G[3,3],F[3,3]
30 E1=2.2E+07
40 E2=1.6E+06
50 G1=6.15E+05
60 V1=0.213
70 V2=0.161
80 Q[1,1]=E1/(1-V1*V2)
90 Q[1,2]=V1*E2/(1-V1*V2)
100 Q[2,2]=E2/(1-V1*V2)
110 Q[3,3]=G1
120 Q[2,1]=Q[1,2]
130 Q[3,1]=0
140 Q[3,2]=0
150 Q[1,3]=0
160 Q[2,3]=0
170 DEG
180 T1=45
190 FOR I=1 TO 2
200 T3=(COS(T1))↑4
210 T4=(SIN(T1))↑2*(COS(T1))↑2
220 T5=(SIN(T1))↑4
230 T6=(SIN(T1))↑4+(COS(T1))↑4
240 T7=SIN(T1)*(COS(T1))↑3
250 T8=(SIN(T1))↑3*COS(T1)
260 R[1,1]=Q[1,1]*T3+2*(Q[1,2]+2*(Q[3,3]))*T4+Q[2,2]*T5
270 R[1,2]=(Q[1,1]+Q[2,2]-4*Q[3,3])*T4+Q[1,2]*T6
280 R[2,1]=R[1,2]
290 L9=Q[1,2]-Q[2,2]+2*Q[3,3]
300 R[1,3]=(Q[1,1]-Q[1,2]-2*Q[3,3])*T7+L9*T8
310 R[2,2]=Q[1,1]*T5+2*(Q[1,2]+2*Q[3,3])*T4+Q[2,2]*T3
320 R[2,3]=(Q[1,1]-Q[1,2]-2*Q[3,3])*T8+L9*T7
330 R[3,1]=R[1,3]
340 R[3,2]=R[2,3]
350 R[3,3]=(Q[1,1]+Q[2,2]-2*Q[1,2]-2*Q[3,3])*T4+Q[3,3]*T6
360 T1=T1*(-1)
370 IF I=2 THEN 440
380 FOR J=1 TO 3
390 FOR K=1 TO 3
400 S[J,K]=R[J,K]
410 NEXT K
420 NEXT J
430 NEXT I
440 H1=0.04
450 H[1]=-0.015
460 H[2]=-0.01
470 H[3]=-0.005
```

```
480 H[4]=0
490 H[5]=0.005
500 H[6]=0.01
510 H[7]=0.015
520 H[8]=0.02
530 FOR I=1 TO 3
540 FOR J=1 TO 3
550 E[1]=Q[I,J]*(H[1]↑3-(-0.02)↑3)
560 E[2]=P[I,J]*(H[2]↑3-H[1]↑3)
570 E[3]=S[I,J]*(H[3]↑3-H[2]↑3)
580 E[4]=Q[I,J]*(H[4]↑3-H[3]↑3)
590 E[5]=Q[I,J]*(H[5]↑3-H[4]↑3)
600 E[6]=S[I,J]*(H[6]↑3-H[5]↑3)
610 E[7]=R[I,J]*(HL7]↑3-H[6]↑3)
620 E[8]=Q[I,J]*(H[8]↑3-H[7]↑3)
630 G[I,J]=(E[1]+E[2]+E[3]+E[4]+E[5]+E[6]+E[7]+E[8])/3
640 NEXT J
650 NEXT I
660 PRINT LIN2
670 DISP "INPUT MX,MY,MXY "
680 INPUT O[1],O[2],O[3]
690 PRINT "FOR MX="O[1]"MY="O[2]"MXY="O[3]
700 PRINT
710 MAT F=INV(G)
720 MAT T=F*O
730 Z9=0.0175
740 MAT F=ZER
750 FOR I=1 TO 3
760 FOR J=1 TO 3
770 P[I]=P[I]+Q[I,J]*(Z9*T[J])
780 NEXT J
790 NEXT I
800 PRINT "OUTERMOST LAYER  X=L  Y=T"
810 PRINT "SIGMA X="P[1]
820 PRINT "SIGMA Y="P[2]
830 PRINT "SIGMA XY="P[3]
840 Z9=0.0125
850 MAT P=ZER
860 FOR I=1 TO 3
870 FOR J=1 TO 3
880 P[I]=P[I]+R[I,J]*(Z9*T[J])
890 NEXT J
900 NEXT I
910 PRINT
920 PRINT "NEXT LAYER          45 DEGS"
930 PRINT "SIGMA X="P[1]
940 PRINT "SIGMA Y="P[2]
950 PRINT "SIGMA XY="P[3]
960 A1=(COS(T1))↑2
970 A2=(SIN(T1))↑2
980 A3=SIN(T1)*COS(T1)
990 A4=(COS(T1))↑2-(SIN(T1))↑2
1000 S1=P[1]*A1+P[2]*A2+P[3]*2*A3
1010 S2=P[1]*A2+P[2]*A1+P[3]*2*A3
```

```
1020 S3=(P[2]-P[1])*A3+A4*P[3]
1030 PRINT
1040 PRINT "SIGMA L="S1
1050 PRINT "SIGMA T="S2
1060 PRINT "SIGMA LT="S3
1070 MAT A=ZER
1080 A[1,1]=E1
1090 FOR I=1 TO 3
1100 FOR J=1 TO 3
1110 E[1]=A[I,J]*(H[1]↑3-(-0.02)↑3)
1120 E[2]=R[I,J]*(H[2]↑3-H[1]↑3)
1130 E[3]=S[I,J]*(H[3]↑3-H[2]↑3)
1140 E[4]=Q[I,J]*(H[4]↑3-H[3]↑3)
1150 E[5]=Q[I,J]*(H[5]↑3-H[4]↑3)
1160 E[6]=S[I,J]*(H[6]↑3-H[5]↑3)
1170 E[7]=R[I,J]*(H[7]↑3-H[6]↑3)
1180 E[8]=A[I,J]*(H[8]↑3-H[7]↑3)
1190 C[I,J]=(E[1]+E[2]+E[3]+E[4]+E[5]+E[6]+E[7]+E[8])/8
1200 NEXT J
1210 NEXT I
1220 MAT F=INV(C)
1230 MAT T=F*Q
1240 MAT P=ZER
1250 FOR I=1 TO 3
1260 FOR J=1 TO 3
1270 P[I]=P[I]+A[I,J]*(Z9*T[J])
1280 NEXT J
1290 NEXT I
1300 PRINT
1310 PRINT "IF E2%G1=0 FOR THE OUTERMOST LAYER, THEN"
1320 PRINT "THE NEXT LAYER WILL EXPERIENCE:"
1330 PRINT "SIGMA X="P[1]
1340 PRINT "SIGMA Y="P[2]
1350 PRINT "SIGMA XY="P[3]
1360 S1=P[1]*A1+P[2]*A2+P[3]*2*A3
1370 S2=P[1]*A2+P[2]*A1+P[3]*2*A3
1380 S3=(P[2]-P[1])*A3+A4*P[3]
1390 PRINT
1400 PRINT "SIGMA L="S1
1410 PRINT "SIGMA T="S2
1420 PRINT "SIGMA TL="S3
1430 GOTO 660
1440 STOP
1450 END
```

```
AN EXAMPLE INPUT
MX=30   MY=20   MXY=10

GIVES THE FOLLOWING OUTPUT



FOR MX= 30   MY= 20   MXY= 10

OUTERMOST LAYER  X=L  Y=T
SIGMA X= 102358.075
SIGMA Y= 34410.8131
SIGMA XY= 12554.31439

NEXT LAYER          45 DEGS
SIGMA X= 24233.75182
SIGMA Y= 37997.41692
SIGMA XY=-4325.568732

SIGMA L= 26730.83565
SIGMA T= 26730.83565
SIGMA LT= 6631.81255

IF E3&G1=0 FOR THE OUTERMOST LAYER, THEN
THE NEXT LAYER WILL EXPERIENCE:
SIGMA X= 35650.03844
SIGMA Y= 58713.63902
SIGMA XY=-10554.46810

SIGMA L= 36627.38063
SIGMA T= 36627.38063
SIGMA TL= 11531.81029
```

LIST OF REFERENCES

1. Linnander, R. J., Laboratory Development and Tensile Testing of Graphite/Glass/Epoxy Hybrid Composite Materials, Masters Degree Thesis, United States Naval Postgraduate School, Monterey, 1974.

2. Air Force Materials Laboratory Contract Report Number F33615-71-C-1362, Advanced Composite Design Guide, by Rockwell International Corporation, January 1973.

3. Jones, Robert M., Mechanics of Composite Materials, p. 147 to 172, McGraw-Hill, 1975.

4. Hanley, D. P., and Cross S. L., Studies Related to the Acoustic Failure Resistance of Advanced Composites, paper presented at Twelfth National SAMPE Symposium "Advances in Structural Composities," Anaheim California, 10-12 October 1967.

5. Schaum, R. T., Development of a Non-Destructive Inspection Technique for Advanced Composite Materials Using Cholesteric Liquid Crystals, Master Degree Thesis, United States Naval Postgraduate School, Monterey, 1976.

6. National Science Foundation Report Number EERC 73-11, SAP IV, by K. Bathe, E. L. Wilson and F. E. Peterson, June 1973.

7. Timoshenko, S., Woinowsky-Krieger, S., Theory of Plates and Shells, p. 364 to 376, McGraw-Hill, 1959.

8. Meirovitch, L., Analytical Methods In Vibrations, p. 179 to 189, MacMillan, 1967.

9. Naval Air Systems Command Report Number NADC-75119-30, Low Velocity Transverse Normal Impact Of Graphite Epoxy Composite Laminates, by E. J. McQuillen, R. E. Llorens and L. W. Gause, 1 December 1975.

10. Grezczuk, L. B., "Response of Isotropic and Composite Materials to Particle Impact," Foreign Object Impact Damage to Composites, ASTM STP 568, American Society for Testing and Materials, p. 183-211, 1975.

11. Colangelo, V. J. and Heiser, F. A., Analysis of Metallurgical Failures, p. p. 113, John Wiley and Sons, 1974.

12. National Advisory Committee for Aeronautics Report TN 1475, Non-linear Large Deflection Boundary Value Problem of Rectangular Plates, by Chi-teh wang, 1948.

INITIAL DISTRIBUTION LIST

		No. Copies
1.	Library, Code 0212 Naval Postgraduate School Monterey, California 93940	2
2.	Department Chairman, Code 67 Department of Aeronautics Naval Postgraduate School Monterey, California 93940	1
3.	Asst. Prof. M. H. Bank, Code 67Bt Department of Aeronautics Naval Postgraduate School Monterey, California 93940	5
4.	Lt. R. L. Ferris, USN 16418 Nordhoff Street Sepulveda, California 91343	1
5.	Defense Documentation Center Cameron Station Alexandria, VA 22314	2